Master of Science Thesis in Electrical Engineering
Department of Electrical Engineering, Linköping University, 2021

A Component-based Model of a Fuel Cell Vehicle System

David Salomonsson & Erik Eng

LINKÖPING UNIVERSITY

Master of Science Thesis in Electrical Engineering

A Component-based Model of a Fuel Cell Vehicle System

David Salomonsson & Erik Eng

LiTH-ISY-EX--21/5394--SE

Supervisor: **Olov Holmer**
ISY, Linköpings universitet
Erik Höckerdal
Scania
Pontus Svens
Scania

Examiner: **Lars Eriksson**
ISY, Linköpings universitet

Division of Automatic Control
Department of Electrical Engineering
Linköping University
SE-581 83 Linköping, Sweden

Abstract

Improving the efficiency and performance of vehicle propulsion systems has always been desirable, and with increasing environmental awareness this has become increasingly topical. A particularly strong focus today is at fossil-free alternatives, and there is a strong trend for electrification. Hybrid powertrains of different types can bring benefits in certain aspects, and there is a lot of research and development involved in the making of a new powertrain.

In this thesis, a complete powertrain for a fuel cell hybrid electric vehicle is modeled, with the intention of contributing to this trend. The model can be used to investigate design choices and their impact on energy consumption. A component-based library is developed, with the purpose of being easy to implement for different configurations.

The results show that it is possible to assemble and simulate a complete hybrid drivetrain, using the modeled components, while not being very computationally heavy. The developed models correspond well with reality, while being modular and easy to implement.

Acknowledgments

This master thesis project has been a great opportunity to apply skills and knowledge acquired over the course of the engineering program at Linköping University. The project has been interesting, challenging and rewarding at the same time.

We therefore would like to sincerely thank Prof. Lars Eriksson, at the Vehicular Systems division at Linköping University, for entrusting and assigning us this project. We are grateful for your commitment, for assisting us with modeling experience, and for the inspiring conversations we have had.

We would like to give a special thanks to our supervisor at Linköping University, Olov Holmer, for all the help and valuable feedback throughout the project, contributing to improving our thesis.

We would also like to give a big thanks to our supervisors at Scania, Pontus Svens and Erik Höckerdal, for their assistance. Your application knowledge and advice on interesting aspects to investigate, along with interesting technical discussions, have been highly appreciated.

Finally, we are also very grateful to our respective families for their support throughout our years of studies.

David Salomonsson, Erik Eng
Linköping, May 2021

Contents

Notation **xi**

1 Introduction **1**
1.1 Objective . . . 1
1.2 Problem Formulation . . . 2
1.3 Outline . . . 2

2 System Description **3**
2.1 Fuel Cell . . . 4
2.1.1 Purge Valve and Recirculation . . . 4
2.2 Complementary Energy Storage . . . 4
2.2.1 Battery . . . 5
2.2.2 Supercapacitor . . . 5
2.3 Traction Motor . . . 5
2.4 Power Electronics . . . 6
2.5 Power Management . . . 6
2.6 Cooling Circuit Auxiliary Components . . . 7
2.6.1 Radiator . . . 7
2.6.2 Bypass Valve . . . 7
2.7 Air Circuit Auxiliary Components . . . 7
2.7.1 Compressor . . . 7
2.7.2 Throttle . . . 8
2.8 Humidifier . . . 8

3 Related work **9**
3.1 Fuel Cell Hybrid System . . . 9
3.2 Fuel Cell . . . 10
3.3 Battery . . . 10
3.4 Supercapacitor . . . 11
3.5 Traction Motor . . . 11
3.6 Power Electronics . . . 12
3.7 Compressor/Blower . . . 12

4 Component Modeling **13**
4.1 Model Assumptions . . . 13
4.1.1 General . . . 14
4.1.2 Fuel Cell . . . 14
4.1.3 Complementary Energy Storage . . . 15
4.1.4 Traction Motor . . . 15
4.1.5 Power Electronics . . . 15
4.1.6 Power Management . . . 15
4.1.7 Air Circuit . . . 16
4.1.8 Cooling System . . . 16
4.1.9 Humidifier . . . 16
4.1.10 Control Volumes . . . 17
4.2 Fuel Cell . . . 17
4.2.1 Mass Flows . . . 17
4.2.2 Voltage and the Polarization Curve . . . 21
4.2.3 Thermodynamics . . . 23
4.2.4 Purge Valve and Recirculation . . . 24
4.3 Complementary Energy Storage . . . 25
4.3.1 Battery . . . 25
4.3.2 Supercapacitor . . . 26
4.4 Traction Motor . . . 28
4.5 Power Electronics . . . 29
4.5.1 DC to AC and AC to DC . . . 29
4.5.2 DC to DC . . . 29
4.6 Power Management . . . 29
4.7 Cooling Circuit Auxiliary Components . . . 30
4.7.1 Pump . . . 30
4.7.2 Bypass Valve . . . 31
4.7.3 Radiator with fan . . . 32
4.8 Air Circuit Auxiliary Components . . . 34
4.8.1 Compressor . . . 34
4.8.2 Throttle . . . 36
4.9 Humidifier . . . 36
4.10 Control Volumes . . . 36

5 Parameter Estimation and Validation **39**
5.1 Mass Flow Estimation in Fuel Cell . . . 39
5.2 Throttle Effective Area Estimation . . . 40
5.3 Compressor Estimation . . . 41
5.4 Efficiency Estimation of Traction Motor . . . 42

6 Model Validation **45**
6.1 Fuel Cell . . . 45
6.1.1 Mass Flows and Humidity . . . 45
6.1.2 Cell Voltage and the Polarization Curve . . . 49
6.1.3 Thermodynamics . . . 50

6.1.4 Purge Valve . . . 51
6.2 Complementary Energy Storage . . . 52
6.2.1 Battery . . . 52
6.2.2 Supercapacitor . . . 54
6.3 Traction Motor . . . 55
6.4 Power Management . . . 56
6.4.1 DC to DC . . . 56
6.5 Air Circuit Auxiliary Components . . . 57
6.5.1 Compressor . . . 57
6.5.2 Throttle . . . 57
6.6 Cooling Circuit Auxiliary Components . . . 58
6.6.1 Radiator with fan . . . 58
6.6.2 Bypass Valve and Pump Validation . . . 59
6.7 Control Volumes . . . 61

7 Simulations **63**
7.1 Ramp Simulation . . . 63
7.2 Drive Cycle Simulation . . . 64

8 Discussion **69**
8.1 Results . . . 69
8.2 Method . . . 70
8.3 The Work in a Broader Perspective . . . 71

9 Conclusions and Future Work **73**
9.1 Conclusions . . . 73
9.2 Future Work . . . 75
9.2.1 Control strategy . . . 75
9.2.2 Improve the power management . . . 75
9.2.3 Benchmark the model . . . 75
9.2.4 Battery capacity & C-rate . . . 75
9.2.5 Liquid Water Formation and Flooding . . . 76
9.2.6 Water Tank, Water Separator and System Water Balance . . . 76
9.2.7 Component Mass . . . 76
9.2.8 More Configurations . . . 76
9.2.9 Fuel Cell Inlet Temperature . . . 77

A Full drive cycle simulation **81**

Bibliography **87**

Notation

Abbreviation

Abbreviation	Meaning
AC	Alternating current
ChL	Choke line
DC	Direct current
EPR	Equivalent parallel resistance
ESR	Equivalent series resistance
FCHEV	Fuel cell hybrid electric vehicle
FCV	Fuel cell vehicle
PEM	Polymer electrolyte membrane
PEMFC	Proton exchange membrane fuel cell
PI	Proportional and integral (regulator)
PID	Proportional, integral, differential (regulator)
QS	Quasistatic
RC	Resistor-capacitor
SoC	State of Charge
SoH	State of Health
ZSL	Zero slope line

Nomenclature

Nomenclature	Meaning
A	Area, m^2
b	Width, m
C	Capacitance, Farad
c	Flow coefficient, -
C_p	Specific heat capacity, J/kgK
D	Diffusion coefficient, m^2/s
E	Energy, J
H	Enthalpy, J
h	Convective heat transfer coefficient, W/m^2K
I	Current, A
k	Thermal conductivity, W/mK
L	Length, m
M	Molar mass, kg/mol
m	Mass, kg
$\dot{m}$	Mass flow, kg/s
N	Number of , -
n_e	Number of electrons per molecule, -
$\dot{n}$	Mass flow of amount of substance, mol/s
P	Power, W
p	Pressure, Pa
Q	Heat energy, J
q	Heat flow, J/s
R	Gas constant, J/mol
R	Resistance, Ω
T	Temperature, K
t	Time, s
U	Voltage, V
u	Absolute humidity, -
v	Volume, m^3
$\dot{v}$	Volume flow, m^3
η	Efficiency, -
λ_a	Excess air ratio, -
λ_h	Excess hydrogen ratio, -
ω	angle speed, rad/s
ϕ	Relative humidity
δ	Thickness, m
ν	Kinematic viscosity, m^2/s
ρ	Density, kg/m^3
Π	Pressure ratio, -

Subscript

Subscript	Meaning
a	Air
act	Activation
amb	Ambient
an	Anode
b	Battery
ca	Cathode
comp	Compressor
conc	Concentration
cond	Conduction
conv	Convection
cool	Cooling
cross	Crossover
del	Delivered
dis	Disturbance
EPR	Equivalent parallel resistance
ESR	Equivalent series resistance
est	Estimation
fc	Fuel cell
gen	Generated
h	Hydrogen
ing	Injection
mbr	Membrane
N	Nitrogen
o	Oxygen
oc	Open circuit
ohm	Ohmic
pur	Purge
r	Reaction
rad	Radiator
rec	Recirculation
req	Required
rev	Reversible
sat	Saturated
sc	Supercapacitor
thr	Throttle
tm	Traction motor
sup	Supply
w	Water

1 Introduction

Electric vehicles are becoming increasingly common. Especially in the passenger car category, but the progress is spreading into heavy-duty vehicles as well. A general concern for the environment is a probable reason for this development, and the pursuit of new and efficient propulsion systems is highly topical today. In particular, much development concerns fossil-free alternatives. The battery as an energy storage method has received much attention. Another contender, which will be focused on in this thesis, is the fuel cell (FC). Particularly, it is the proton exchange membrane fuel cell (PEMFC), which uses hydrogen as the energy carrier, that will be used in this thesis. The supercapacitor can also be utilized in an electric propulsion system. Each of these has their advantages and disadvantages in relation to each other. There exists multiple models around this topic but they mainly focus on some aspect of the fuel cell or a subsystem, and not the whole system. The models that cover the whole system tend to be considerably simplified. More on this in Chapter 3. A vehicle that uses a fuel cell in combination with a battery and/or supercapacitor is known as a fuel cell hybrid electric vehicle (FCHEV). A general term for any vehicle with fuel cells is fuel cell vehicle (FCV).

1.1 Objective

The objective of this thesis is to model a propulsion system for an FCV. The model can be used to investigate design choices and their impact on energy consumption, or performance in general. The model is component based, meaning that it aims at being easy to set up, covering any hybrid configuration and dimensioning according to the wishes of the user. The FCV system consists of several subsystems, and is dependent on several auxiliary components, each of which

is modeled individually. Being modular, the FCV system model should also be easy to implement to existing vehicle models having other propulsion systems. In particular, this model is implemented and tested with the model of a heavy duty truck described in [8]. The truck model is modified merely by replacing the diesel engine subsystem with the FCV system developed in this thesis.

1.2 Problem Formulation

This thesis will handle the modeling of fuel cells, with surrounding associated subsystems. The main focus will be to build up a component library, perform parameter estimation, and make necessary control systems. The model database will be an extension to an existing vehicle model using an internal combustion engine; the truck benchmark model from [8].

Questions that should be answered are:

- What subsystems need to be modeled, and how will they connect and interact?
- What level of model complexity is sensible for the system and subsystems?
- How well do the models correspond to reality, and how are they validated?

1.3 Outline

A short description of each chapter is presented below.
Chapter 2, System Description
Theory for each component is presented.
Chapter 3, Related Work
Discussion about related work is presented.
Chapter 4, Component Modeling
Equations and models are presented for each component.
Chapter 5, Parameter Estimation and Validation
Parameter estimation is validated and presented.
Chapter 6, Model Validation
All the models are validated.
Chapter 7, Simulation
Results for a driving scenario for the complete hybrid powertrain model is presented.
Chapter 8, Discussion
Discussion about results and method is presented.
Chapter 9, Conclusion
Problem formulations are answered as well as future work.

2

System Description

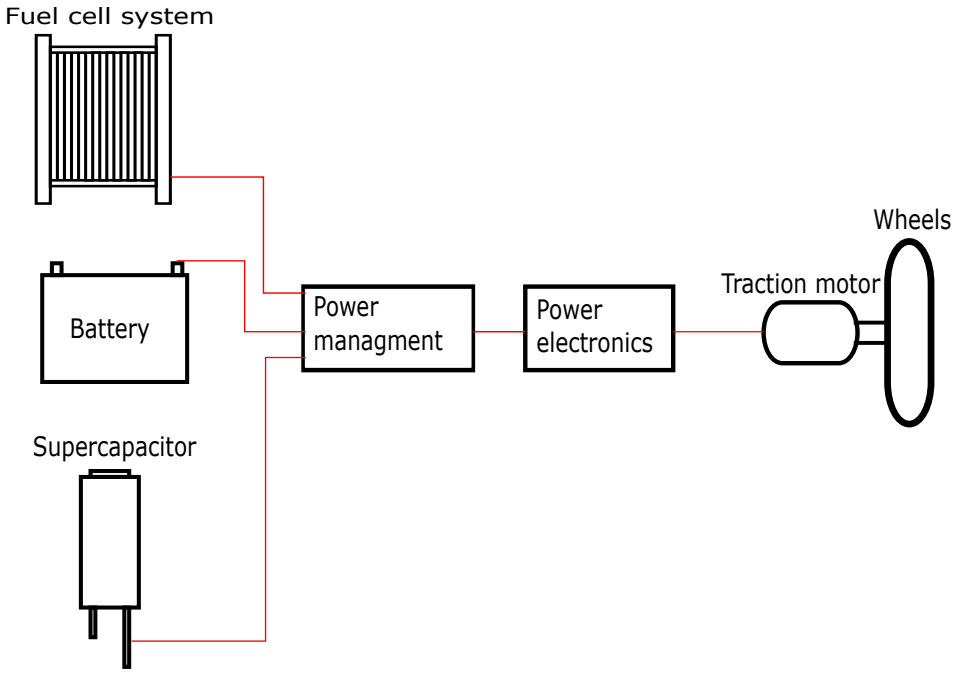

Figure 2.1: *Sketch of the electric powertrain. Fuel cell system refers to the fuel cell along with its auxiliary components.*

2.1 Fuel Cell

There are several types of fuel cells. The fuel cell in this thesis is a proton exchange membrane fuel cell (PEMFC), which uses hydrogen as fuel. The fuel reacts with oxygen, creating electricity, heat and water. It has an anode including a plate with channels that fuel flows through, and a similar plate with channels at the cathode that air flows through. Separating the electrodes is a so called polymer electrolyte membrane (PEM), and catalyst layers on each side of the membrane. The membrane prevents the crossing of electrons, but allows the crossing of protons. At the anode, the catalyst causes hydrogen gas (H_2) to split into protons, or hydrogen ions (H^+), and electrons (e^-). A concentration gradient arises between the two sides of the membrane, and as a consequence of this, hydrogen ions diffuse through the membrane to the cathode. At the cathode, the catalyst causes the oxygen gas (O_2) to split into free oxygen atoms, and stick to the surface of the catalyst. The electrodes are connected with a conductor, having the electrical circuit, and load, of the system in between. The positively charged ions now on the cathode side leads to a current from the anode to the cathode, through the conductor. As the electrons can pass through the conductor to the cathode, the oxygen reacts with the hydrogen ions to form water (H_2O), and the course of reaction is complete [10].

Several fuel cells may be connected in series, forming a stack. The fuel cell stack in this system is utilized as a range extender, complementing a battery pack, although supercapacitors may be included in the system too. The aim is to run the fuel cell stack mainly at favorable operating conditions. Excess and deficit of power production will be covered by the battery and/or supercapacitors, leading to either charging or discharging of these.

2.1.1 Purge Valve and Recirculation

In many fuel cells the hydrogen is recirculated to increase the fuel efficiency of the stack. However, this creates a problem since the membrane not only lets the hydrogen through, but also the nitrogen from the air side to the hydrogen side. This creates a contamination effect in the recirculated fuel, which needs to be purged. This is often done by a control valve called the purge valve. Normally the purge valve is opened at around 25% concentration of nitrogen on the hydrogen side [19].

2.2 Complementary Energy Storage

In this section, the battery and the supercapacitor as additional means of energy storage and conversion, that can complement the fuel cell in a hybrid configuration, is presented. The implementation of either of these components can complement the operation of a fuel cell, in the sense of covering up the difference in power requirement in case of rapid changes. By doing so, the possibility to keep the fuel cell around its optimal operating point is improved. The battery

can also contribute as an additional external energy source, considering that it can be charged, and store energy, between driving occasions. Figure 2.1 shows a principle sketch of the implementation of complementary energy storage.

2.2.1 Battery

Batteries represent an energy storage system, that can convert stored chemical energy into electrical energy. The reverse is also true, such that electrical energy can be converted and stored as chemical energy. The former applies while the battery is discharging under load, and the latter while the battery is charging. While a battery could be designed to meet certain requirements for a relatively high amount of energy storage, the main source of energy in an FCHEV is the stored hydrogen for the fuel cell. A lithium-ion battery has, in relation to hydrogen gas, very low energy density and specific energy. Although, in addition to the increased amount of energy storage a battery amounts to, a battery makes possible recuperative braking. Also, batteries generally have higher specific power than what a fuel cell can deliver [36].

2.2.2 Supercapacitor

A supercapacitor is an energy storage system, and can either be used in combination with the battery and the fuel cell, or as the only complement to the fuel cell, in a hybrid configuration. The supercapacitor has two electrodes separated by an electrolyte and an insulating membrane. The energy stored is a result of the charge separation taking place between the electrodes. Reducing the distance between the electrodes increases the capacity, and extending the surface area of the electrodes is another mean to increase the capacity. A supercapacitor differs from a conventional capacitor in the materials of which it is made. In terms of the difference in performance, a supercapacitor generally has slightly lower specific power, but much higher specific energy, or capacitance. A conventional capacitor has far too low specific energy for being useful in a vehicle propulsion system, which makes the supercapacitor the favorable type of capacitor for this purpose. In relation to the battery though, a supercapacitor typically has higher specific power, and lower specific energy [31]. The ability to handle higher power means that recuperative braking can be taken advantage of to a greater extent, if used in combination with a battery. If no battery is present, supercapacitors enable recuperative braking without one. However, the lower specific energy and faster self-discharge, compared with batteries, makes them unfit for long-term energy storage [34].

2.3 Traction Motor

The traction motor converts electric energy into torque and speed. There exist many different kinds of traction motors, but the ones mostly used in the car industry are the ones driven by an AC source.

2.4 Power Electronics

Power electronics are the electronic components responsible for changing the current either from AC to DC or from DC to AC. A DC to DC converter is also considered a part of this class. All these converters works by controlling the current with diodes and switches.

2.5 Power Management

When a battery and/or a capacitor is complemented to the fuel cell system, power management is of need. This system calculates the operating points for each component in relation to the current required from the system.

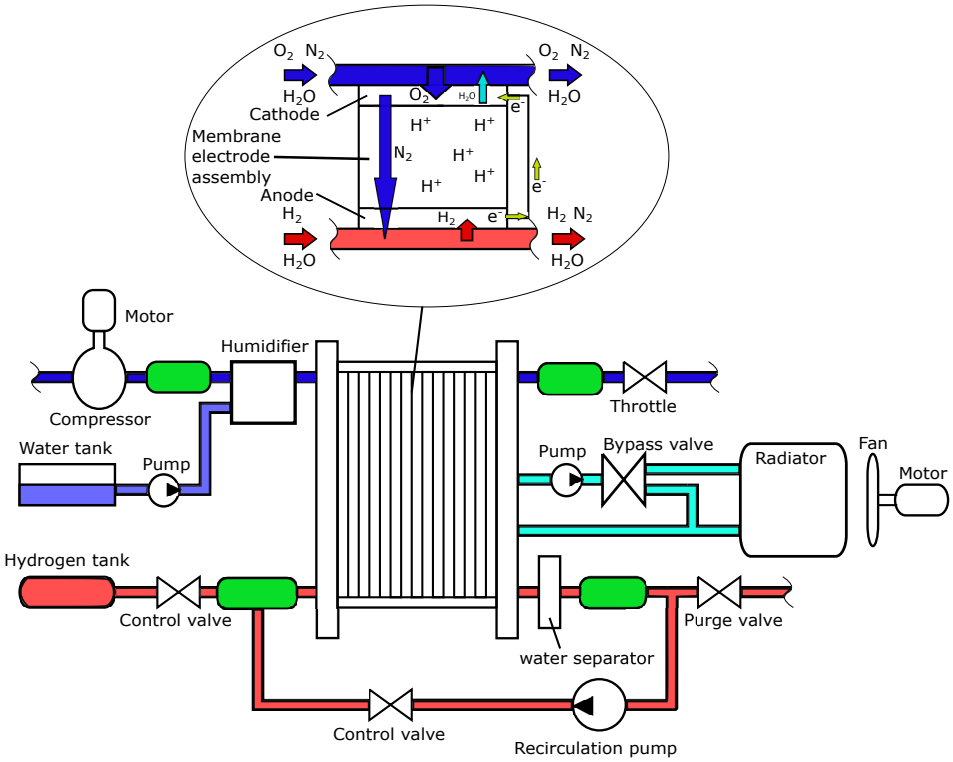

Figure 2.2: *Sketch of the fuel cell system. Dark blue is the air circuit while red is the hydrogen circuit. Cyan is the cooling circuit. The green boxes are the control volumes.*

2.6 Cooling Circuit Auxiliary Components

The cooling circuit cools the fuel cell to a reference temperature to make sure the fuel cell runs optimally. There exist many different cooling configurations, but a standard configuration is a pump with a radiator. In some cases a bypass valve is also added for better temperature control. A configuration for a coolant system can be seen in Figure 2.2.

2.6.1 Radiator

The radiator is the component where the majority of the heat dissipation occurs. It first transfers the heat from the coolant to the radiator fins, and then from the fins to the air. How much heat a radiator can transfer depends mainly on how much heat that is transferred from the coolant to the fins and then to the air. This heat dissipation is done by convection, conduction, and radiation. The heat convection can be further divided into forced and natural convection, where the forced convection is a function of the fluid/gas speed.

2.6.2 Bypass Valve

The bypass valve is a control valve that redirects the flow in the system depending on the temperature. If cooling is needed a part of the flow is directed to the radiator, otherwise it is bypassed. This helps the system to reach the reference temperature faster. A configuration with a bypass valve can be seen in Figure 2.2.

2.7 Air Circuit Auxiliary Components

The air circuit is one of the major systems responsible for supplying the fuel cell with air for the chemical process. The air circuit can be configured in multiple ways, but the most common is that a blower or compressor supplies the fuel cell with air. There are also in some cases a control valve, or a throttle, after the fuel cell to act as a pressure regulator to the fuel cell.

2.7.1 Compressor

The compressor used in this thesis is a centrifugal compressor and is used to supply the fuel cell system with the required airflow. The compressor can also work with a control valve to build extra pressure inside the system.

The compressor map has three main operating regions, the map region, the surge region and the choke region. The map region is where the compressor normally works at and are separated from, the surge region by the zero slope line (ZSL) and the choke region by the choke line (ChL).

The surge region is where the mass flow becomes unstable because of too high pressure ratio over the compressor. In this region, the pressure ratio tends to be high, which can lead to negative mass flow, limiting the pressure that can be

generated. There is also a possibility to damage the compressor in this region because of the high pressure ratio. The choke region is where the maximum flow is achieved because of the sonic condition called choking.

2.7.2 Throttle

A throttle is a control valve that limits the mass flow. The mass flow can be controlled by changing the throttle plate angle, which in turn can be used to build pressure.

2.8 Humidifier

The proton conductivity in the PEM has a great influence on the performance of the fuel cell, and it is highly dependent on the water content in the membrane. A higher water content promotes the conductivity, and a lower water content lowers the conductivity. The humidity levels, and thus the membrane water content, varies with operating conditions in the fuel cell. For this reason, an external humidifier can be considered for the system, adding the possibility to supply water and the ability to raise the humidity levels inside the fuel cell [25]. Several types of humidifiers exist, and a review is made in [13].

3
Related work

In general, most components can be modeled according to two main approaches, Quasistatic (QS) and dynamic modeling. The QS approach offers very low complexity but gets less accurate to the reality since it does not model dynamics. The dynamic approach on the other hand tend to include the dynamic behavior of systems, but leads to a higher complexity. A common approach is to start with fundamentals, and then add more dynamics gradually.

3.1 Fuel Cell Hybrid System

A model of a fuel cell hybrid electric vehicle (FCHEV), with configuration in series, is presented in [4]. The system is composed of a fuel cell stack, a DC-DC converter and a supercapacitor. The fuel cell stack is modeled with a static empiric model. The DC-DC converter is modeled using simple mathematical operations, while efficiencies for the converter is retrieved from experimental data. The supercapacitor is modeled using equivalent RC-circuits.

In [30], some existent FCHEVs are reviewed in terms of performance. To do this, a model of a FCHEV is derived, and vehicle-specific parameters are used. All modeling of the subsystems is kept relatively simple, using QS approach. Hence dynamics are ignored, and efficiencies are also estimated to be constant.

The consequences, and possible fuel savings, of optimizing battery size for a fuel cell stack are investigated in [11]. A power management strategy for FCHEVs, utilizing a battery in addition to the fuel cell stack, is also presented.

In [26], an FCHEV using both battery and supercapacitors combined with the fuel cell stack is regarded. Similarly to [11], the aim of this article is to optimize

the sizing of the involving components, with respect to system efficiency and fuel economy. A power management strategy is proposed as well.

3.2 Fuel Cell

The fuel cell in itself is a complex system to model, with many dependencies, but it can be simplified and adapted depending on what the aim of the model is. According to [29], it is often sufficient to reproduce the polarization curve with a polynomial function. A method to create the polynomial function, with low computation cost, would be to interpolate from measured data of a fuel stack. This method gives the option to include the effect of different membrane or flow fields [29]. More detailed approaches to modeling of the polarization curve, with losses are presented in [10, 14–16, 29]. In [14, 29] a detailed approach, with dynamics for the the fuel cell is presented. In [15, 16], two models are presented, the 1-D and 2-D quasi models. In [10], a dynamic model and a 1-D QS model is presented. In general, all the fuel cell associated models presented in [10, 14–16, 29] are detailed and well explained.

3.3 Battery

In [10, p. 114], it is suggested that a basic model for a battery can be derived by considering an equivalent circuit of the system, consisting of an ideal open-circuit voltage source in series with an internal resistance. It is stated that this approach applies for both QS modeling and dynamic modeling, although the equivalent circuit differs slightly between the two cases. For dynamic modeling, the internal resistance is elaborated and split into several components [10, p. 123]. The mathematical model for the QS model is attained by using Kirchhoff's voltage law on the equivalent circuit. The same applies for the dynamic modeling, although Kirchhoff's current law is used too, forming a differential equation in addition to the first equation [10, pp. 122-123]. A dynamic battery model derived from an equivalent circuit is also used in [32]. The internal resistance is slightly simplified compared to the one in [10, p. 123].

The open-circuit voltage of a battery is dependent on the state of charge (SoC) and temperature. In [10, p. 114], the dependency of open-circuit voltage on SoC is modeled using an affine relationship in SoC. This applies to both QS- and dynamic modeling. The dependency on temperature is omitted. In [32], the influence on voltage of both SoC and temperature is taken into account, using a polynomial. The coefficients of the polynomial are determined from experimental data. In [24], the influence of SoC is ignored.

[10], [32] and [24] each present a similar battery thermal model, as energy balance equations. They have in common being derived lumped models from electrochemical models. Another property shared between the models is that they take into account two contributions to heat generation in the battery, namely

ohmic resistance and polarization resistance. Lastly, they all also make the assumption that the heat is perfectly distributed within the battery, treating it as a single reservoir. [32] analyzes the impact on performance the operating temperature and applied current has on lithium-ion batteries. Here it is also investigated what dependence the model parameters have on both temperature and current. In [24], the focus lies solely on the impact of operating temperature on the performance of lithium-ion batteries. This paper also proposes a cooling strategy for batteries.

[10, p. 125], [32] and [24] all bring up that purely electrochemical models can accurately predict the dynamic behavior of a battery. Furthermore, all three sources point out that electrochemical models are particularly computational heavy when applied to fast simulation or control design, and not suitable for this purpose.

Battery size optimization in a fuel cell vehicle propulsion system is investigated in [11]. The paper also proposes an energy management strategy between the fuel cell and the battery with the traction motor.

3.4 Supercapacitor

In [34], it is claimed that supercapacitors are commonly modeled using electrochemical models or equivalent circuit models. Equivalent circuit models are depicted as resistor-capacitor (RC) networks of varying extents. A more complex network, i.e. a larger number of series and/or parallel connections, usually leads to higher accuracy at the cost of computational efficiency. [30] dives deeper into this, and presents the influence the number of series- and parallel connections has on the equivalent capacitance. In [34], dynamic mathematical expressions are derived from the equivalent circuit using Kirchhof's circuit laws. Thermal modeling, and the phenomenon of self-discharge, are also brought up in this paper.

3.5 Traction Motor

In [10, p. 87-104], there is both a QS model, and a dynamic model, for the traction motor. The QS approach provides a simple power approach while the dynamic approach takes resistance and inductance as well as motor control into consideration. A similar model as described in the dynamic approach is described in [35]. The dynamic approach can be hard to model since a controller for the motor need to be implemented. There are also many parameters that needs to be known by the designer which makes the model more complex.

3.6 Power Electronics

A converter from DC to AC, called an inverter, tends to be complex if all the dynamic behaviors are to be considered. A simpler approach is only to consider the losses. The losses can be modeled according to [9], however this model can be relatively complex as well.

A converter from AC to DC, or rectifier, tends to have its losses tied with the rectification ratio. A method to calculate the rectification ratio is presented in [17]. However this method needs some electric modeling.

A converter from DC to DC, tends to be a big system with many sub-components. An approach to avoid to model all these sub-models are presented in [5].

3.7 Compressor/Blower

A well-defined model for a fuel cell blower and an approach for the control of the fuel cell blower is presented in [13]. The formula takes into consideration the inertia of both the blower and the motor. The efficiency is defined as constant in the model but can be expanded. A model for both a dynamic and QS approach is presented in [10], which is more complex than [13]. Lastly, a model for a compressor is presented in [20–22]. All these models have in common the need of a compressor/blower map.

4

Component Modeling

In this chapter, the modeling of each subsystem will be presented and motivated. Model assumptions are also listed.

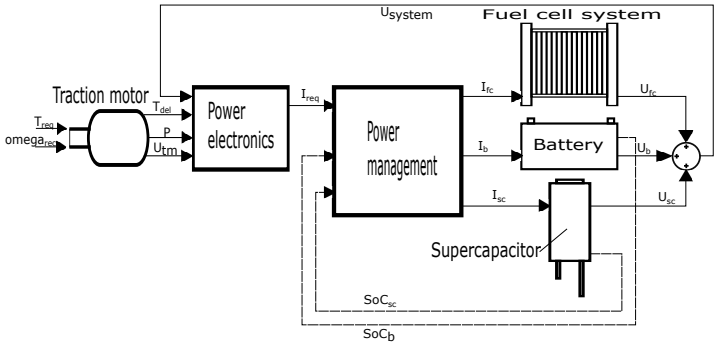

Figure 4.1: *Sketch of how the signals are connected in the electric powertrain. Fuel cell system refers to the whole fuel cell system with cooling, air and hydrogen circuits.*

4.1 Model Assumptions

The scope of this thesis has been adapted according to the time plan of 20 weeks and relevance. The model assumptions are listed below, and may be discussed further in the corresponding chapters.

4.1.1 General

The general assumptions for our models are listed below.

- Heat losses to the environment between subsystems, in transmission lines or pipes in general, are assumed to be zero
- Pressure drops between subsystems, in transmission lines or pipes in general, is assumed to be zero
- Component mass is ignored
- No temperature change over restrictor valves
- No optimization of the system is considered; simple control strategy is applied, and not carefully tuned

4.1.2 Fuel Cell

The assumptions concerning the fuel cell are listed below.

- The temperature is assumed to be perfectly spread among the fuel cells in the stack, and between cathode and anode
- Pressure drop over the fuel cell for air, hydrogen, and water is assumed to be linear in relation to the mass flow and pressure
- The temperature of the exhaust gases is assumed to be equal to the fuel cell temperature
- The mass flow of gases through the fuel cell is assumed to be linearly dependent on the pressure difference
- The mix of partial pressures of gases in the fuel cell is not regarded for the voltage model; instead, a constant partial pressure of 21% of oxygen in the cathode and 100% of hydrogen on the anode is assumed
- The fuel cell is not affected by the inlet temperature of the gas, in anode and cathode

Purge Valve

- Water concentration is not taken into consideration when partial pressure is calculated
- The nitrogen concentration is not modeled when the purge is open, since it will decrease to zero when the pressure stabilises in the anode system
- No leakage when the valve is closed
- No consideration to what pressure difference that exist over the cell when the purge occurs

4.1.3 Complementary Energy Storage

The assumptions concerning the battery and the supercapacitor are listed below.

Battery

- Temperature is disregarded
- Constant, perfect, State of Health (SoH)
- Internal resistances are not dependent on SoC, temperature or SoH
- Coulombic efficiency is disregarded, and assumed to be 100%
- The battery capacity is not dependent on current, and thus not dependent on the C-rate

Supercapacitor

- Temperature is disregarded

4.1.4 Traction Motor

The assumptions concerning the traction motor are listed below.

- No electronic components are modeled
- Instant torque delivery
- Constant voltage over motor

4.1.5 Power Electronics

For all the power electronic components, no detailed modeling has been done, because of the complexity it gives to the model and also that the focus of this thesis is on the fuel cell. Also, both the DC to AC and AC to DC -converters are modeled as a QS system with a static loss that comes from the efficiency. The DC to DC is also assumed to have a perfect regulator that tunes the parameter D. The output voltage to the traction motor is also assumed to be constant because of the modeling approach.

4.1.6 Power Management

The assumptions concerning the power management are listed below.

- No implementation for a configuration with both fuel cell, capacitor and battery

4.1.7 Air Circuit

The assumptions concerning the air circuit are listed below.

- The fluid passing the throttle is assumed to be a compressible fluid
- Compressor works as a poorly designed turbine when the flow is negative
- No multi-variable control strategy is used to regulate the pressure inside the cathode independent of the mass flow

4.1.8 Cooling System

The assumptions concerning the cooling system are listed below.

- No pressure and heat loss in the pipes outside of the radiator, since the length is often unknown
- The pump is ideal with no dynamic because a dynamic pump adds extra complexity with minor performance improvement
- The Reynolds number is calculated at the end of the fins, where in reality, the Reynolds number varies across the fins. This is to simplify the modeling of the Reynolds number as well as it is the worst-case scenario
- No flow analysis was done on how the air flows in the radiator. Hence the flow was assumed to be constant across the whole radiator
- The bypass valve has no leakage when fully closed or open since data for the bypass valve was hard to find
- The radiator has been estimated to only deliver heat to the environment by conduction and convection since they deliver the majority of heat transfer to the environment in a radiator
- The fan power consumption is assumed to depend linearly on the flow
- Fan power consumption does not depend on the surrounding air temperature or pressure

4.1.9 Humidifier

- No dynamics of any pump or heating/vaporization is taken into account. The mass flow of injected water is controlled directly, meaning that the response is fully dependent on the control parameters, and can be made arbitrarily quick
- The humidifier does not consume power
- No water tank is regarded, and an infinite amount of water is available

4.1.10 Control Volumes

The assumptions concerning the control volumes are listed below.

- The gas is a perfect gas
- No gas dynamic
- Constant temperature in the control volume
- Complete and immediate mixing of gases

4.2 Fuel Cell

The modeling of the fuel cell is divided into four main categories; mass flows, voltage, thermodynamics, and purge valve.

4.2.1 Mass Flows

The mass flow model is in turn divided into three submodels; the cathode model with its main object to manage the air mass flows, the anode model with its main object to manage the hydrogen mass flows, and the model for the membrane water activity, where humidity levels also are managed. All equations concerning the cathode and anode mass flows are retrieved from [10].

Cathode mass flows

For each mole of hydrogen converted, half a mole of oxygen is needed

$$\dot{n}_o(t) = \frac{1}{2}\dot{n}_h(t) \tag{4.1}$$

where $\dot{n}_o(t)$ is the mass flow of amount of substance of oxygen, and $\dot{n}_h(t)$ is the mass flow of amount of substance of hydrogen. The requirement on oxygen mass flow for the reaction in the stack is in turn dependent on the fuel cell current, $I_{fc}(t)$, as

$$\dot{m}_{o,r}(t) = \frac{NI_{fc}(t)M_o}{2n_eF} \tag{4.2}$$

where N is the number of fuel cells in series, M_o the molar mass of oxygen, n_e the number of electrons per molecule, F the Faraday constant. This relationship is strictly according to electrochemistry. Although in practice, a stack operates with excess air, a ratio denoted by $\lambda_a(t) > 1$, and thus the required mass flow of air-based on the reaction can be estimated as

$$\dot{m}_{a,in,r}(t) = \lambda_a(t)\frac{NI_{fc}(t)M_o}{2n_eF}\frac{100}{21} \tag{4.3}$$

The reason for operating with excess air is because of a concentration gradient of oxygen arising along the membrane, decreasing further away from the inlet, as it is consumed in the reaction. A mass fraction of oxygen in the inlet air of 21% is assumed. In actuality, the mass flow rate of air is a result of the pressure drop over the cathode channel, as well as the fuel cell current, according to

$$\dot{m}_{a,in} = K_a(p_{ca,in}(t) - p_{ca,out}(t)) + \frac{1}{2}\dot{m}_{o,r}(t) \tag{4.4}$$

where K_a is an estimation parameter for the level of flow restriction. The inlet and outlet pressure of the cathode, $p_{ca,in}$ and $p_{ca,out}$, are managed by the air circuit auxiliary component models, presented in Section 4.8, in combination with the thermodynamic control volumes presented in Section 4.10.

The mass flow of water entering the cathode is expressed as

$$\dot{m}_{w,ca,in}(t) = u_0\dot{m}_{a,in}(t) + \dot{m}_{w,inj}(t) \tag{4.5}$$

where u_0 is the absolute humidity in the ambient air, and $\dot{m}_{w,inj}(t)$ is the mass flow of water injected by the humidifier, which is also the control signal for the humidity control. The mass flow of water exiting the cathode is

$$\dot{m}_{w,ca,out}(t) = \dot{m}_{w,ca,in}(t) + \dot{m}_{w,gen}(t) + \dot{m}_{w,mbr}(t) \tag{4.6}$$

where $\dot{m}_{w,gen}(t)$ is the water production rate inside the cathode as a result of the cell reaction, and $\dot{m}_{w,mbr}(t)$ is the rate of water flux through the membrane, described more in detail in Section 4.2.1. The water production rate is evaluated as

$$\dot{m}_{w,gen}(t) = \dot{m}_{h,r}(t)\frac{M_w}{M_h} \tag{4.7}$$

Anode mass flows

The mass flow of hydrogen needed for the reaction, strictly electrochemically, is a function of $I_{fc}(t)$, and given by

$$\dot{m}_{h,r}(t) = \frac{NI_{fc}(t)M_h}{n_eF} \tag{4.8}$$

Just as for the mass flow of air on the cathode side, and for the same reason, a certain amount of excess hydrogen is desired to be kept on the anode side, represented by $\lambda_h > 1$ in the following equation

$$\dot{m}_{h,in}(t) = \lambda_h\frac{NI_{fc}(t)M_h}{n_eF} \tag{4.9}$$

Part of the anode inlet mass flow is from the hydrogen tank, and part is recirculated from the outlet back to the inlet, as follow

$$\dot{m}_{h,in}(t) = \dot{m}_{h,rec}(t) + \dot{m}_{h,tank}(t) \tag{4.10}$$

Nitrogen in the air may cross the membrane, and contaminates the fuel doing so. Therefore, the outlet mass flow needs to be purged at times. The amount of fuel recirculated is thus given by

$$\dot{m}_{h,rec}(t) = \dot{m}_{h,out}(t) - \dot{m}_{h,pur}(t) \tag{4.11}$$

The actual mass flow of hydrogen is a consequence of the pressure difference over the anode, according to

$$\dot{m}_{h,in}(t) = K_h(p_{an,in}(t) - p_{an,out}(t)) + \frac{1}{2}\dot{m}_{h,r}(t) \tag{4.12}$$

The pressures $p_{an,in}(t)$ and $p_{an,out}(t)$ are determined using the control volumes presented in Section 4.10.

The mass flow of water entering the anode is given by

$$\dot{m}_{w,an,in}(t) = \dot{m}_{h,tank}(t)u_{an,tank} + \dot{m}_{w,an,out}(t) \tag{4.13}$$

where $u_{an,tank}$ is the absolute humidity of the fuel stored in the tank, usually assumed to correspond to a relative humidity of 100% [10]. The water contained in the recirculated exhausts is included in this equation. The mass flow of water exiting the anode is given by

$$\dot{m}_{w,an,out}(t) = \dot{m}_{w,an,in}(t) - \dot{m}_{w,mbr}(t) \tag{4.14}$$

taking into account the membrane water flux.

Membrane water activity and humidity levels

The humidity levels inside the fuel cell have a substantial influence on the performance of the fuel cell. In general, the humidity can be expressed as a function of pressure and temperature, as [10]

$$u = \frac{M_w}{M_a}\frac{\phi p_{sat}(\vartheta)}{p - \phi p_{sat}(\vartheta)} \Leftrightarrow \phi = \frac{puM_a}{(uM_a + M_w)p_{sat}(\vartheta)} \tag{4.15}$$

where u is absolute humidity, ϕ is relative humidity, and M_w and M_a the molar mass of water and air, respectively. p_{sat} is the saturation pressure of water vapour, and is a function of air temperature expressed as [12]

$$p_{sat}(\vartheta) = \frac{exp\left(34.494 - \frac{4924.99}{\vartheta + 237.1}\right)}{(\vartheta + 105)^{1.57}}, \quad (\vartheta > 0°\mathrm{C}) \tag{4.16}$$

The humidity levels at the inlet and outlet stages of the cathode and anode are given by Equations (4.17-4.20) [10].

$$u_{ca,in}(t) = \frac{\dot{m}_{w,ca,in}(t)}{\dot{m}_{a,in}(t)} \quad (4.17) \qquad u_{an,in}(t) = \frac{\dot{m}_{w,an,in}(t)}{\dot{m}_{h,in}(t)} \quad (4.19)$$

$$u_{ca,out}(t) = \frac{\dot{m}_{w,ca,out}(t)}{\dot{m}_{a,out}(t)} \quad (4.18) \qquad u_{an,out}(t) = \frac{\dot{m}_{w,an,out}(t)}{\dot{m}_{h,out}(t)} \quad (4.20)$$

$u_{ca}(t)$ and $u_{an}(t)$ can be approximated as the average of the inlet and outlet humidity levels, and can be inserted into Equation (4.15) to obtain ϕ_{ca} and ϕ_{an}. The rate of water flux through the membrane is evaluated as [10]

$$\dot{m}_{w,mbr} = M_w N \left(n_d \frac{I_{fc}(t)}{F} - A_{fc} D_w \frac{\phi_{ca}(t) - \phi_{an}(t)}{\delta_{mbr}} \right) \quad (4.21)$$

where A_{fc} is the fuel cell active area, and δ_{mbr} is the membrane thickness. The remaining subsequent equations, up to and including Equation (4.26), are retrieved from [18]. n_d is the electro-osmotic drag coefficient, dependent on the membrane water content, λ_{mbr}, and is expressed as

$$n_d = 0.0029\lambda_{mbr}^2 + 0.05\lambda_{mbr} - 3.4 \cdot 10^{-19} \quad (4.22)$$

D_w is the diffusion coefficient, expressed as

$$D_w = D_\lambda exp\left(2416\left(\frac{1}{303} - \frac{1}{T_{fc}}\right)\right) \quad (4.23)$$

where D_λ also is a function of membrane water content as

$$D_\lambda = \begin{cases} 10^{-6} & , \lambda_{mbr} < 2 \\ 10^{-6}(1 + 2(\lambda_{mbr} - 2)) & , 2 \leq \lambda_{mbr} \leq 3 \\ 10^{-6}(3 + 1.67(\lambda_{mbr} - 3)) & , 3 \leq \lambda_{mbr} \leq 4.5 \\ 1.25 \cdot 10^{-6} & , \lambda_{mbr} \geq 4.5 \end{cases} \quad (4.24)$$

The membrane water content is evaluated according to

$$\lambda_{mbr,i} = \begin{cases} 0.043 + 17.81a_i - 39.85a_i^2 + 36a_i^3 & , 0 < a_i \leq 1 \\ 14 + 1.4(a_i - 1) & , 1 < a_i \leq 3 \end{cases} \quad (4.25)$$

$$a_i = \frac{p_{v,i}}{p_{sat,i}} \quad , i \in [an, ca] \quad (4.26)$$

and can be calculated for either the anode and the cathode, as appears from the equations. Although, the mean value of the membrane water content is calculated using the mean value of a_{ca} and a_{an}.

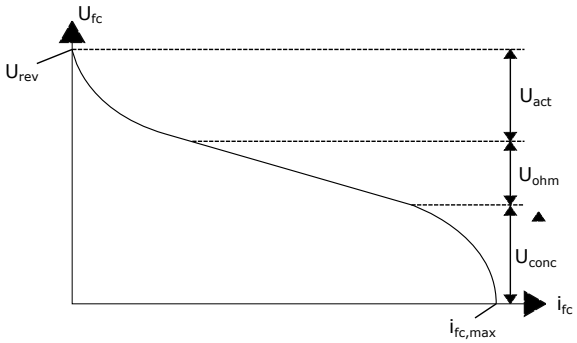

Figure 4.2: *A typical appearance of a polarization curve, revealing what polarization is dominant at what fuel cell current density.*

4.2.2 Voltage and the Polarization Curve

The upper limit of what voltage is attainable by a fuel cell is given by the equilibrium potential, often referred to as reversible cell potential, U_{rev}. The reversible cell potential is a function of fuel cell temperature and partial pressures of reactants, but is otherwise constant with respect to the current. The actual cell voltage is affected by irreversible losses, or polarizations, generally presumed to consist of three main contributions; activation polarization, $U_{act}(t)$, ohmic polarization, $U_{ohm}(t)$, and concentration polarization, $U_{conc}(t)$. Each of these losses has a primary influence on the fuel cell voltage at different fuel cell current densities, visualized in Figure 4.2. For the visualization of the polarization curve, all other operating variables are kept constant, while the current is ramped. The current density, $i_{fc}(t)$, is indicated along the x-axis, and is defined as [10]

$$i_{fc}(t) = \frac{I_{fc}(t)}{A_{fc}} \tag{4.27}$$

The polarizations also depend on the fuel cell temperature, humidity, and operating pressure, although the combined effect of varying these is complex. That is why, for the simulation of a polarization curve, these operating parameters are kept constant. The total fuel cell voltage for a single cell, $U_{fc,cell}(t)$, is summarized into [10]

$$U_{fc,cell}(t) = U_{rev} - U_{act} - U_{ohm} - U_{conc} \tag{4.28}$$

The reversible cell voltage is [27]

$$\begin{aligned} U_{rev} = {} & 1.229 - 8.5 \cdot 10^{-4}(T_{fc} - 298.15) \\ & + 4.3085 \cdot 10^{-5} T_{fc} \left[\ln(p_{H_2}) + \frac{1}{2} \ln(p_{O_2}) \right] \end{aligned} \tag{4.29}$$

where p_{H_2} and p_{O_2} are the partial pressures of hydrogen and oxygen. The activa-

tion polarization is [27]

$$U_{act}(t) = (c_0 + v_a(1 - e^{-c_1 i})) \quad , \quad c_1 = 10 \tag{4.30}$$

where c_0 and v_a are given by Equations (4.31) and (4.32). p_{ca} is the cathode pressure, assumed to be the average of the inlet and outlet cathode pressure.

$$\begin{aligned} c_0 = {} & 0.279 - 8.5 \cdot 10^{-4}(T_{fc} - 298.15) \\ & + 4.3085 \cdot 10^{-5} T_{fc} \left[\ln\left(\frac{p_{ca} - p_{sat}}{1.01325} + \frac{1}{2} \ln\left(\frac{0.1173(p_{ca} - p_{sat})}{1.01325} \right) \right) \right] \end{aligned} \tag{4.31}$$

$$\begin{aligned} v_a = {} & (-1.618 \cdot 10^{-5} T_{fc} + 1.618 \cdot 10^{-2}) \left(\frac{p_{O_2}}{0.1173} + p_{sat} \right)^2 \\ & + (1.8 \cdot 10^{-4} T_{fc} - 0.166) \left(\frac{p_{O_2}}{0.1173} + p_{sat} \right) \end{aligned} \tag{4.32}$$

The ohmic polarization is given by Equation (4.33). The ohmic resistance, R_{ohm}, is defined as the ratio between the thickness of the membrane, δ_{mbr}, and the membrane conductivity, σ_{mbr}, as [27]

$$U_{ohm} = I_{fc}(t) R_{ohm} \tag{4.33}$$

$$R_{ohm} = \frac{\delta_{mbr}}{\sigma_{mbr}} \tag{4.34}$$

The membrane conductivity is a function of the fuel cell temperature and the membrane water content according to [27]

$$\begin{aligned} \sigma_{mbr} &= (b_{11} \lambda_{mbr} - b_{12}) exp\left(b_2 \left(\frac{1}{303} - \frac{1}{T_{fc}} \right) \right) \\ b_{11} &= 0.05139 \\ b_{12} &= 0.00326 \\ b_2 &= 350 \end{aligned} \tag{4.35}$$

where b_{11} and b_{12} are membrane specific parameters, in this case for Nafion 117. b_2 is a parameter to be adjusted to fit fuel cell data. The concentration polarization is [27]

$$U_{conc} = (i_{fc} \left(c_2 \frac{i_{fc}}{i_{fc,max}} \right)^{c_3} \tag{4.36}$$

and c_2 and c_3 is given by Equations (4.37) and (4.38) [27].

$$c_2 = \begin{cases} (8.66 \cdot 10^{-5} T_{fc} - 6.80 \cdot 10^{-2})(\frac{p_{O_2}}{0.1173} + p_{sat}) + \\ (-1.60 \cdot 10^{-4} T_{fc} + 0.539) & , \frac{p_{O_2}}{p_{sat}} + 0.1173 \geq 2atm \\ \\ (7.16 \cdot 10^{-4} T_{fc} - 0.622)(\frac{p_{O_2}}{0.1173} + p_{sat}) + \\ (-1.45 \cdot 10^{-3} T_{fc} + 1.68) & , else \end{cases} \tag{4.37}$$

$$c_3 = 2 \tag{4.38}$$

The voltage of the stack is the product of the fuel cell voltage for a single cell and the number of cells connected in series,

$$U_{fc}(t) = U_{fc,cell}(t)N \tag{4.39}$$

and the power of the stack is attained by multiplying with the fuel cell current,

$$P_{fc}(t) = U_{fc,cell}(t)NI_{fc}(t) = U_{fc}(t)I_{fc}(t) \tag{4.40}$$

4.2.3 Thermodynamics

The temperature of the fuel cell stack can be evaluated by the energy balance as follows [18]:

$$M_{fc}C_{fc}\frac{dT_{fc}}{dt} = q_{gen}(t) - q_{conv}(t) - q_{cool}(t) \tag{4.41}$$

where M_{fc} is the mass of the stack, C_{fc} is the heat capacity of the stack, and $M_{fc}C_{fc}$ forms the thermal mass of the fuel cell stack. q_{gen} is the heat generated by the stack, given by

$$q_{gen}(t) = I_{fc}(t)(U_{id} - U_{fc,cell}(t))N \tag{4.42}$$

U_{id} is the "caloric voltage", defined as in Equation (4.43), which denotes the voltage that would be achieved by a total conversion of enthalpy into electrical energy. This voltage is, in practice, impossible to reach.

$$\begin{aligned} U_{id} &= -\frac{\Delta H}{n_e F} \\ \Delta H &= -285.9[MJ/kmol] \end{aligned} \tag{4.43}$$

where ΔH is the heating value of the reaction. The convective heat transfer is given by

$$q_{conv} = k_{conv}A_{st}(T_{fc} - T_{amb}) \tag{4.44}$$

where k_{konv} is the heat transfer coefficient for the stack, A_{st} is the external surface

area of the stack, and T_{amb} is the ambient temperature. q_{cool} is the heat dissipated by the coolant, as

$$q_{cool} = \dot{m}_{cool} c_{p,cool} (T_{cool,out} - T_{cool,in}) \tag{4.45}$$

where $\dot{m}_{cool}$ is the mass flow of the coolant, $c_{p,cool}$ is the heat capacity of the coolant, $T_{cool,out}$ and $T_{cool,in}$ is the outlet and inlet temperature of the coolant. The outlet temperature of the coolant is assumed to coincide with the fuel cell temperature [18]. The voltage efficiency of a fuel cell is defined as [10]

$$\eta_{V,fc}(I_{fc}) = \frac{U_{fc,cell}(I_{fc})}{U_{rev}} \tag{4.46}$$

and the electrochemical Carnot efficiency, which takes into account that not all the heating value can be converted into useful work, is defined as [10]

$$\eta_{id} = \frac{-\Delta G}{-\Delta H} = \frac{U_{rev}}{U_{id}} \tag{4.47}$$

where ΔG represents the Gibbs free energy. Another efficiency, based on excess hydrogen, is also presented in [10]. This however is not included in this model because of the recirculation, which negates this factor. In [10], a system efficiency is also presented, which takes into consideration auxiliary power consumption. The efficiency concerning the fuel cell in this thesis does not include this, and thus the fuel cell efficiency is given by

$$\eta_{fc}(I_{fc}) = \eta_{V,fc}(I_{fc})\eta_{id} = \frac{U_{fc,cell}(I_{fc})}{U_{rev}} \frac{U_{rev}}{U_{id}} = \frac{U_{fc,cell}(I_{fc})}{U_{id}} \tag{4.48}$$

4.2.4 Purge Valve and Recirculation

The purge valve is modeled as a restricting valve with a constant K_{pur}. This constant correlates to the relation between the mass flow the valve lets through and the pressure difference. K_{pur} is estimated based on data. The purge valve is also modeled with a constant α_{pur} that stand for how much the valve is open or closed, $\alpha_{pur} = [0, 1]$.

$$\dot{m}_{pur} = \alpha_{pur} K_{pur} (p_{b,pur} - p_{amb}) \tag{4.49}$$

To calculate the nitrogen concentration α_{N_2}, the diffusion between the anode and cathode side needs to be determined. According to experimental results, this crossover rate depends on the temperature, water uptake, and membrane thickness [2]. A proposed equation for the crossover rate as a function of the crossover constant, k_{cross}, is presented in [19]. However, this equation has many unknowns that are not normally known, or hard to model. Instead, an experimental plan to determine this constant can be used. The method to estimate this constant is presented in [19].

With the crossover coefficient known, the nitrogen concentration can be deter-

mined as [19]

$$\dot{\alpha}_{N_2} = c_1 - c_2 \alpha_{N_2} \tag{4.50a}$$

$$c_1 = \frac{R T_{an} k_{cross} p_{N_2,ca}}{V_{an} p_{an}} \tag{4.50b}$$

$$c_2 = \frac{R T_{an} k_{cross}}{V_{an}} \tag{4.50c}$$

where T_{an} is the temperature out from the stack, V_{an} the volume of the anode side and p_{an} the outlet pressure of the anode side.

4.3 Complementary Energy Storage

4.3.1 Battery

The battery model used is derived from a dynamic equivalent circuit, and is known as Randles model [10, pp. 122-123]. In this equivalent circuit, the battery is represented by an ideal open-circuit voltage source, U_{oc}, in series with a resistance being the ohmic overpotential, R_o, and two parallel branches following in series. On one of the two parallel branches, two resistances are in series. These are the diffusion overpotential, R_d, and the charge-transfer overpotential, R_{ct}. On the opposite branch, the capacitive current flows through a double-layer capacitance, C_{dl}. Every equation presented in this battery section is derived from [10].

Voltage & state of charge

Using Kirchhoff's voltage and current laws, dynamic equations for the battery voltage, U_b, are yielded as

$$\begin{aligned} U_b(t) &= U_{oc} - R_o I_b(t) - U_o(t) \\ R_o C_{dl} \frac{d}{dt} U_o(t) &= U_{oc} - U_b(t) - U_o(t) \left(1 + \frac{R_o}{R_d + R_{ct}}\right) \end{aligned} \tag{4.51}$$

where U_o represents the non-ohmic overpotential that applies over the parallel branches. R_o, R_d, R_{ct} and C_{dl} are specified parameters, while $U_b(t)$ and $U_o(t)$ are the unknown variables solved by the equation system. The open-circuit voltage of the battery represents the equilibrium potential. It is a function of the battery SoC, and may be estimated by an affine relationship as

$$U_{oc}(t) = \kappa_2 \xi_b(t) + \kappa_1 \tag{4.52}$$

where $\xi_b(t)$ is the state of charge, given by the ratio

$$\xi_b(t) = \frac{X(t)}{X_0} \tag{4.53}$$

where $X(t)$ is the present battery electric charge, and X_0 is the battery capacity.

The variation of the battery charge is proportional to the battery current, and can be approximated as

$$\dot{X}(t) = -I_b(t) \tag{4.54}$$

In Simulink, the SoC is computed as

$$\xi_b(t) = \frac{X_{init}}{X_0} + \frac{1}{3600}\int -I_b(t)\,dt \tag{4.55}$$

based on Equations (4.53) and (4.54), where the ratio between X_{init} and X_0 states the initial battery charge at the start of the simulation. The current is defined as positive for discharging, and negative for charging.

Thermodynamics

The overall efficiency of a battery can be modeled in several different ways, with different levels of complexity. The suitability of each efficiency model may depend on the application and objectives of the battery model. One alternative, which has the advantage of being entirely based on the present operating conditions, is [10, p. 120]

$$\eta_b = \begin{cases} \frac{U_b}{U_{oc}} & , I \geq 0 \\ \frac{U_{oc}}{U_b} & , I < 0 \end{cases} \tag{4.56}$$

which is a preferred way of estimating efficiency for use in supervisory controllers [10, Ch. 7]. Since the voltage levels are dependent on the current and SoC, the efficiency is as well. All losses following the overall efficiency is considered to be lost as heat, leading to the heat generation being implemented as

$$q_b(t) = (1 - \eta_b)U_b|I_b| \tag{4.57}$$

4.3.2 Supercapacitor

Similarly, as for the battery model, the model of the supercapacitor is derived from an equivalent circuit. A supercapacitor has non-linear behavior, and this can be accounted for in an equivalent circuit by a certain number of parallel resistance-capacitor-branches, with different time constants. The more parallel branches included, the more accurate imitation of the non-linear behavior is possible. The supercapacitor can really be represented by infinitely many different varieties of equivalent circuits, with varying complexity. The equivalent circuit chosen to represent the supercapacitor is one presented in [23], consisting of a resistance in series with one pair of a parallel branch, having a resistance on one branch, and a capacitance, C, on the other. The resistance in series with the two branches is denoted equivalent series resistance (ESR), and the resistance on one of the branches is denoted equivalent parallel resistance (EPR). This equivalent circuit is simple, but accurate, even though it does not fully reflect the non-linear behavior. The precision loss is small. It covers self-discharging, through the

branch with the EPR, which is substantial for a supercapacitor.

Voltage & state of charge

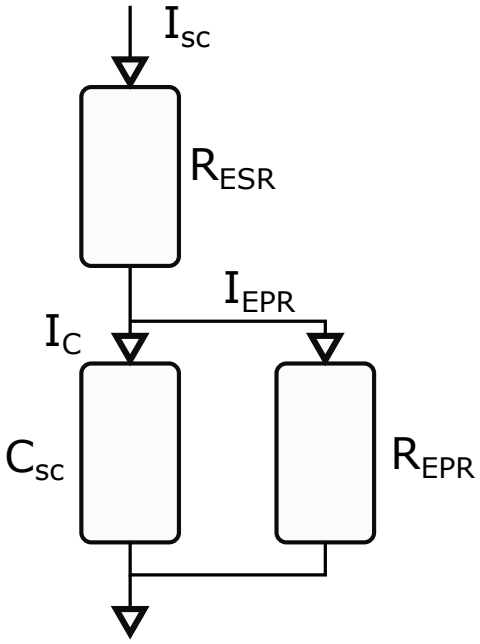

Figure 4.3: *The equivalent circuit of the supercapacitor*

The supercapacitor is modeled according to an equivalent circuit presented in [4]. A sketch of this circuit is presented in Figure 4.3, where I_{sc} is the current input to the capacitor, I_{EPR} the current that goes through the equivalent parallel resistance and I_C the current that goes through the capacitor. The current that goes through the equivalent parallel resistance is determined by

$$I_{EPR} = \frac{U_{EPR}}{R_{EPR}} = \frac{1}{C_{sc}} \int I_C \tag{4.58}$$

where C_{sc} is the capacitance of the supercapacitor. The current over the capacitor is then determined by

$$I_C = I_{sc} - I_{EPR} \tag{4.59}$$

With the currents known the voltage over the circuit can be describes as

$$U_{sc} = I_{sc} R_{ESR} + \frac{1}{C_{sc}} \int I_C \tag{4.60}$$

The energy stored by a supercapacitor is given by [30]

$$E_{sc}(t) = \frac{1}{2} C_{sc} U_{sc}^2(t) \tag{4.61}$$

and the maximum amount of energy a supercapacitor can store is given by [30]

$$E_{sc,max}(t) = \frac{1}{2} C_{sc} U_{sc,max}^2(t) \tag{4.62}$$

The SoC of a supercapacitor is defined as the ratio between what stored energy remains and the maximum amount of energy it can store [30],

$$\xi_{sc}(t) = \frac{E_{sc}(t)}{E_{sc,max}} = \frac{U_{sc}^2(t)}{U_{sc,max}^2} \tag{4.63}$$

Thermodynamics

A global efficiency of a supercapacitor is established based on a full charge/discharge cycle, under the condition of either constant current (Peukert test) or at constant power (Ragone test). The global efficiency is then defined as the ratio of the energy delivered during a full discharge to the energy required for a full charge. However, the efficiency of a supercapacitor can also be defined locally, based on a power ratio rather than an energy ratio. This has the advantage of not being based on any assumptions on the conditions during charging and discharging. The local efficiency of a supercapacitor is defined as [10, Ch. 4.6.2]

$$\eta_{sc}(I_{sc}) = \frac{P_d}{|P_c|} = \frac{U_{sc}C_{sc} - R_{ESR}C_{sc}|I_{sc}|}{U_{sc}C_{sc} + R_{ESR}C_{sc}|I_{sc}|} \tag{4.64}$$

where P_d and P_c is the power during discharge and charge, respectively. The heat generation is based on the efficiency, under the assumption that all energy lost leads to heat, as

$$q_{sc} = (1 - \eta_{sc}) U_{sc} |I_{sc}| \tag{4.65}$$

4.4 Traction Motor

In [10, p. 87-103], a QS and a dynamic approach are presented. The quasistatic approach models the motor simply by the power flow, while the dynamic approach goes into more detail with motor control and more. The approach that this thesis motor model was based on is mainly the quasistatic approach with some aspect from the dynamic approach.

The model to simulate the traction motor is based on that the output power is equal to the input plus the losses. The losses are equal to the estimated power consumption, $P_{TM,est}$ minus the input power.

$$P_{in} = T_{tm}\omega_{tm} \tag{4.66a}$$

$$P_{tm} = P_{in}(T_{tm}, \omega_{tm}) + P_{loss}(T_{tm}, \omega_{tm}) \tag{4.66b}$$

$$P_{loss}(T_{tm}, \omega_{tm}) = P_{TM,est}(T_{tm}, \omega_{tm}) - P_{in}(T_{tm}, \omega_{tm}) \tag{4.66c}$$

where T_{tm} and ω_{tm} is the requested torque and speed. $P_{TM,est}$ is estimated according to data and a function for it is presented in Chapter 5.

4.5 Power Electronics

The modeling of the power electronics are divided into converter between AC and DC and DC voltage converters.

4.5.1 DC to AC and AC to DC

These converters are hard to model because the behavior of each sub electronic component that it consists of, need to be modeled as well. Because of this complexity, the converters are modelled according to a QS approach with only the efficiency η. The efficiency is also considered to be constant. With this, a function for how the power out is affected by the power in can be expressed as

$$P_{out} = \frac{P_{in}}{\eta} \tag{4.67}$$

4.5.2 DC to DC

The DC to DC converter is modeled as a Bidirectional boost converter which can work for both normal propulsion and regeneration braking. It operates as a normal boost converter when driving and as a buck converter when regeneration braking. The DC voltage transfer function for this converter when in boost mode is presented in [5] as

$$\frac{V_{in}}{V_{out}} = \frac{1}{1-D} \tag{4.68a}$$

$$\eta = \frac{R(1-D)^2}{R(1-D)^2(1+V_D/V_{out}+fC_0R)+r_l} \tag{4.68b}$$

$$\eta = \frac{P_{out}}{P_{inp}} = \frac{V_{out}I_{out}}{V_{in}I_{in}} \tag{4.68c}$$

where V_D is the forward conduction voltage drop of the diode, C_0 is the output capacitance of the switch, r_l is the ESR of the inductor and the term fC_0R represents switching losses in the converter. The term D represents how much the DC to DC need to regulate. When the vehicle is operating in buck the efficiency is estimated to be constant.

4.6 Power Management

The power management can be modeled according to many principles, depending on what is of interest. Often the efficiency of the fuel cell is of particularly high interest since it is the subsystem that is most affected by its operating point. Thus it can have the greatest impact on system efficiency. A method to achieve high system efficiency is by using the battery/capacitor as a short time storage buffer that takes care of quick changes in load and then use the fuel cell as long time supplier of power. One method to do this is to regulate the state of charge of the battery/capacitor while switching operating points for the fuel cell. With

this, it is possible to limit the fuel cell load fluctuation while still supplying the motor with enough power. How the power management interacts with the other systems is visualized in Figure 4.1.

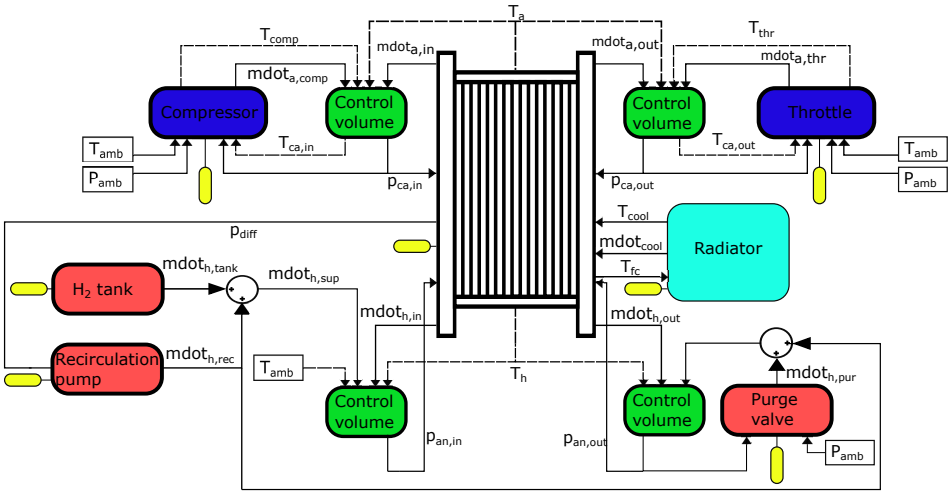

Figure 4.4: *Sketch of how the signals are connected in the fuel cell system. Dark blue is the air circuit, while red is the hydrogen circuit and cyan is the cooling circuit. The green boxes are the control volumes. Every yellow box illustrates a possible regulator that can control the subsystems.*

4.7 Cooling Circuit Auxiliary Components

The cooling system in this thesis is made of a pump, a bypass valve, and a radiator with a fan. The main component is the radiator that cools the circuit. A sketch of how the cooling circuit is integrated with the fuel cell system is presented in Figure 4.4.

4.7.1 Pump

The pump is modeled as a ideal system with a regulator that controls the flow. Hence the only model that is needed is a model for how the power consumption is related to the mass flow and pressure difference in the system. The pressure difference is calculated by considering the pressure losses in the radiator and the fuel cell. The pressure loss in the radiator is estimated to only depend on the bends and the friction in the pipes. A model for the pressure losses due to friction and pipe bends are presented in [6]. The model for the friction takes into consideration the density ρ and speed of the fluid v. The model also takes into consideration the length L and the diameter d of the pipes.

$$\Delta p_f = \lambda \frac{l \rho v^2}{2} \tag{4.69}$$

where λ is the friction factor which is determined by

$$\lambda = \frac{64}{Re} \quad , Re \leq 2300 \tag{4.70}$$

$$\lambda = \frac{0.316}{\sqrt[3]{Re}} \quad , 2300 < Re < 10^5 \tag{4.71}$$

The losses in pressure due to the bend are also dependent on the speed and density as well as a factor ζ. The parameter ζ depends on the angle of the pipe φ and the constant ζ_{90} which can be determined by Table 4.1. d in the table is the diameter of the pipe while r is the radius of the bend.

$$\Delta p_{dis} = \zeta \frac{\rho v^2}{2} \tag{4.72}$$

Table 4.1: *Pipe bend single loss factor. Taken from [6]*

d/r	0.2	0.4	0.6	0.8	1
ζ_{90}	0.13	0.14	0.16	0.21	0.29

The pressure loss in the fuel is modeled as a linear restrictor with a constant K which is determined by data.

$$\Delta p = \frac{\dot{m}}{K} \tag{4.73}$$

With all the pressure losses in the system, the power consumption can be express as [10, p. 247]

$$P = \frac{\dot{m}\Delta p}{\rho \eta} \tag{4.74}$$

where $\dot{m}$ is the mass flow from the pump, Δp pressure difference, ρ density of the fluid and η the efficiency.

4.7.2 Bypass Valve

The bypass opening is assumed to be linear with a term k that stands for the opening for the redirection. k has a value between 0 and 1 where 0 stands for that the flow bypass the radiator and 1 stand for that all the flow goes into the radiator. With this, a function for the temperature before the fuel cell T_{cool}, can be expressed as a function of the fuel cell temperature T_{fc}, the temperature out of the radiator T_{rad}, and k [3].

$$\dot{m}_{rad} = k\dot{m}_{cool} \tag{4.75}$$

$$\dot{m}_{bypass} = (1-k)\dot{m}_{cool} \tag{4.76}$$

$$\dot{m}_c C_{p,cool} T_{cool} = (1-k)\dot{m}_{cool} C_{p,cool} T_{FC} + k\dot{m}_{cool} C_{p,cool} T_{rad} \tag{4.77}$$

where $\dot{m}_{rad}$ is the flow to the radiator while $\dot{m}_{bypass}$ is the flow that bypasses the radiator.

4.7.3 Radiator with fan

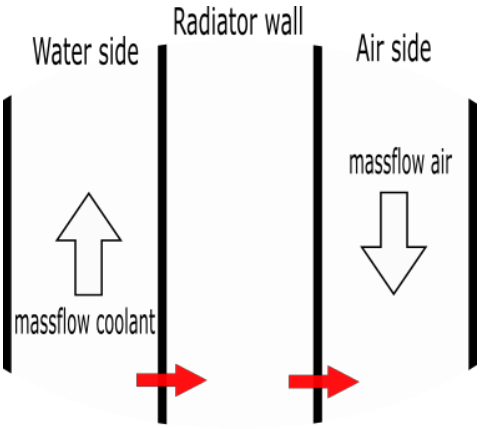

Figure 4.5: *Sketch of a radiator wall*

The radiator is modeled by assuming that the majority of the heat is transferred by the convection and conduction of the radiator. A sketch for how the heat transfers through the system is presented in Figure 4.5.

The conduction can be calculated according to

$$q_{cond} = k_{rad} A_{cond} \frac{dT}{dx} \approx k_{rad} A_{cond} \frac{\Delta T_{cond}}{\Delta x} \tag{4.78}$$

where A_{cond} is the area of the radiator where conduction occurs, k_{rad} is the thermal conductivity of the radiator material, ΔT_{cond} is the temperature differences between the surface temperatures, and Δx is the thickness of the material.

The convection can be calculated according to

$$q_{conv} = h_i A_{conv} \Delta T_{conv} \tag{4.79}$$

where h_i are know as the convective heat transfer coefficient and depends on the speed of the medium i and A_{conv} is the area where convection occurs. ΔT_{conv} is the temperature differences between the surface and the fluid.

The heat transfer is divided into three steps. First the heat transfer from the coolant to the inner wall,

$$q = h_{cool} A_{cool} (T_{fc} - T_{innerwall}) \tag{4.80}$$

then the conduction through the material

$$q = k_{rad} A_{rad} \frac{T_{innerwall} - T_{fins}}{\delta_{wall}} \tag{4.81}$$

and lastly the convection from the fins to the air

$$q = h_a A_a (T_{fins} - T_{air}) \tag{4.82}$$

With all this known one can solve for q and get

$$q = \frac{\Delta T}{\frac{1}{A_{cool} h_{cool}(\dot{m}_{cool})} + \frac{\delta_{wall}}{A_{rad} k_{rad}} + \frac{1}{A_a h_a(\dot{m}_a)}} \tag{4.83}$$

where A_{rad} is the surface area of the radiator and δ_{wall} is the thickness of the radiator. A_a is the area where convection to the air occur and is calculated according to the length L_{fins} and width b_{fins} of the fins as well as the number of fins. The number of side for each fin as well as that the outer fins only have one side is also taken into consideration in Equation (4.84).

$$A_{air} = L_{fins} b_{fins} 2(N_{fins} - 1) \tag{4.84}$$

The area A_{cool} is estimated by taking the lateral surface area of the pipes A_{lat} and multiple the number of pipes N_{pipes} that can fit inside the radiator. The air gap between each pipe is also taken into consideration by the variable $t_{air,gap}$.

$$A_{col} = N_{pipes} A_{lat} \tag{4.85}$$

$$N_{pipes} = \frac{H_{rad}}{D_{pipes} + t_{air,gap}} \tag{4.86}$$

where H_{rad} is the height of the radiator and D_{pipes} is the pipe diameter.

Estimation of h_{cool} and h_{air}

To estimate the convective heat transfer the non-dimensional number, Prandtl(Pr), Nusselt (Nu), and Reynold(Re) are used. The Prandlt number is defined as the ratio of momentum diffusivity to thermal diffusivity.

$$Pr = \frac{\nu \rho C_p}{k} \tag{4.87}$$

where ν is the kinematic viscosity, ρ is the density, C_p specific heat and k is the thermal conductivity. The Reynolds number tells if the medium is turbulent or laminar. Reynold's number is defined as the ratio between internal forces and viscous forces.

$$Re = \frac{vL}{\nu} \tag{4.88}$$

where v is the speed and L is the characteristic length. Nussel is the ratio between the convective and the conductive heat transfer.

$$Nu = \frac{h_x L}{k} \tag{4.89}$$

where h is the convective heat transfer coefficient of the fluid/gas. Nussel can also be estimated based on data, as a function of Pr and Re. This can be used to estimate h based on Nu and Pr. However there exist multiple estimated functions for this. The one modeled in this thesis for the coolant is the Dittus-Boelter equation and for the air an equation presented in [33]. The values for both these

methods can be seen in Table 4.2.

$$Nu = N_1 Re^{N_2} Pr^{N_3} \tag{4.90}$$

Table 4.2: *Parameter value for Equation (4.90)*

	N_1	N_2	N_3
Coolant	0.023	0.8	0.4
Air (Re $<5 \cdot 10^5$)	0.664	$\frac{1}{3}$	0.5
Air ($5 \cdot 10^5 \leq Re \leq 10^7$)	0.037	0.8	$\frac{1}{3}$

Fan

The fan is modeled to only depend on a variable $u_{rad,on}$, which determines how much flow the fan should supply.

$$\dot{m}_{fan} = u_{rad,on} \dot{m}_{fan,max} \tag{4.91}$$

The power is also modeled to depend linearly on $u_{rad,on}$. This variable is regulated by a controller to turn on if the temperature reaches a certain threshold. The signal can vary between 0 and 1.

$$P_{fan} = u_{rad,on} P_{fan,max} \tag{4.92}$$

4.8 Air Circuit Auxiliary Components

The air circuit modeling is divided into a compressor model and a throttle model. Both these models are presented below. A sketch of how the air circuit is integrated with the fuel cell system is presented in Figure 4.4.

4.8.1 Compressor

The compressor is modeled according to [20–22]. In [22] an Ellipse model is used to estimate the flow out from the compressor. The ellipse model defines a relation between the rotational speed, mass flow, and pressure ratio for the compressor. The ellipse model presented in [22] has four different operation regions.

The first region where a compressor normally works at is between the ZSL and ChL. In this region the speed lines are modeled according to an ellipse function [22]

$$\left(\frac{\bar{\dot{m}}_c - \bar{\dot{m}}_{ZS}}{\bar{\dot{m}}_{Ch} - \bar{\dot{m}}_{ZS}} \right)^{CUR} + \left(\frac{\Pi_c - \Pi_{Ch}}{\Pi_{ZS} - \Pi_{Ch}} \right)^{CUR} = 1 \tag{4.93}$$

where $\bar{\dot{m}}_{Ch}$, $\bar{\dot{m}}_{ZS}$, Π_{ZS} and CUR are base parameters that defines the position of the modeled speed lines in the compressor map. All these models depend on the

corrected speed and 14 model parameters, $C_{x,i}$, that need to be estimated[22].

$$\bar{\dot{m}}_{Ch}(\bar{N}_{c,n}) = \bar{\dot{m}}_{c,max}(C_{\dot{m}ch,1} + C_{\dot{m}ch,2}\arctan(C_{\dot{m}ch,3}\bar{N}_{c,n} - C_{\dot{m}ch,4})) \tag{4.94a}$$

$$\Pi_{Ch}(\bar{N}_{c,n}) = \Pi_{c,max}(C_{\Pi ch,1} + C_{\Pi ch,2}\bar{N}_{c,n}^{C_{\Pi ch,3}}) \tag{4.94b}$$

$$\bar{\dot{m}}_{ZS}(\bar{N}_{c,n}) = \bar{\dot{m}}_{c,max}(C_{\dot{m}zs,1}\bar{N}_{c,n}^{C_{\dot{m}zs,2}}) \tag{4.94c}$$

$$\Pi_{ZS}(\bar{N}_{c,n}) = 1 + (\Pi_{c,max} - 1)C_{\Pi zs,1}\bar{N}_{c,n}^{C_{\Pi zs,2}} \tag{4.94d}$$

$$CUR(\bar{N}_{c,n}) = C_{cur,1} + C_{cur,2}\bar{N}_{c,n}^{C_{cur,3}} \tag{4.94e}$$

where the corrected speed is:

$$\bar{N}_{c,n} = \frac{\bar{N}_c}{\bar{N}_{c,max}} \tag{4.95}$$

The second region is below the ChL. In this region, the model is assumed to be vertical line.

The third zone is between zero flow line and the ZSL. In this region, a third degree polynomial function is used to model the pressure ratio.

$$\Pi = \Pi_{c,0} + 3\frac{\Pi_{ZS} - \Pi_{c,0}}{\bar{\dot{m}}_{zs}}\bar{\dot{m}}_{el}^2 - 2\frac{\Pi_{ZS} - \Pi_{c,0}}{\bar{\dot{m}}_{zs}}\bar{\dot{m}}_{el}^3 \tag{4.96}$$

where $\bar{\dot{m}}_{el}$ is an artificial mass flow that is introduced to add flexibility to the shape of the function, and $\Pi_{c,0}$ is the pressure ratio when the flow is zero.This artificial flow and pressure ratio can be described as

$$\bar{\dot{m}}_{el} = \bar{\dot{m}}_{ZS}\left(1 - \left(1 - \frac{\bar{\dot{m}}_c}{\bar{\dot{m}}_{ZS}}\right)^{C_s}\right)^{\frac{1}{C_s}} \tag{4.97}$$

$$\Pi_{c,0}(\bar{N}_{c,n}) = \Pi_{ZS}(\bar{N}_{c,n}) - \Gamma_{\Pi_{cs}}(\Pi_{ZS}(\bar{N}_{c,n}) - 1) \tag{4.98}$$

where the parameter C_s in Equation (4.97) is estimated from data. In the case of $C_s = 1$, $\bar{\dot{m}}_{el} = \bar{\dot{m}}_c$ is identical. The parameters $\Gamma_{\Pi_{cs}}$ in Equation (4.98) is a tuning parameter and can, if surge measurement is available, be adjusted to the desired map. If surge measurement is not available, $\Gamma_{\Pi_{cs}}$ can be set to 1/2 [22].

The final region is negative flow, in this region the compressor is modeled as a poorly designed turbine. Where the pressure ratio is defined as

$$\Pi_c = (\Pi_{c,0} - 1) + \left(1 - \left(\frac{-\bar{\dot{m}}_c}{K_0\bar{\dot{m}}_{c,max}}\right)^2\right)^{-1/K_t} \tag{4.99}$$

where K_0 and K_t are model parameters. The area is normally not measured, and if this is the case, the parameters are set to 0.3 and 2 respectively [22].

4.8.2 Throttle

The throttle is modeled according to an isentropic flow, with no temperature change over the restriction. With this, the mass flow can be calculated as [7]

$$\dot{m} = \frac{p_{us}}{\sqrt{RT_{us}}} A_{eff}(\alpha)\Psi(\Pi) \tag{4.100}$$

where R is the air gas constant, p_{us} upstream pressure and T_{us} upstream temperature. $\Psi(\Pi)$ is a function of the pressure ratio Π if choking is not present, i.e. sonic conditions are not reached in the throat. If choking is reached, $\Psi(\Pi_{lim})$ is a function of the critical value when choking occurs Π_{crit}[7]

$$\Psi(\Pi) = \sqrt{\frac{2\gamma}{\gamma - 1}\left(\Pi_{lim}(\Pi)^{\frac{2}{\gamma}} - \Pi_{lim}(\Pi)^{\frac{\gamma+1}{\gamma}}\right)} \tag{4.101}$$

$$\Pi_{lim}(\Pi) = max\left(\Pi, \Pi_{crit}\right) \tag{4.102}$$

$$\Pi_{crit} = \left(\frac{2}{\gamma + 1}\right)^{\frac{\gamma}{\gamma-1}} \tag{4.103}$$

$$\Pi = \frac{p_{ds}}{p_{us}} \tag{4.104}$$

where γ is the specific heat ratio of air and p_{ds} downstream pressure. The function $A_{eff}(\alpha)$ is estimated according to data and considers the air leakage when the throttle is closed by the term A_0 and how the effective area depends on the throttle plate angle α_{th} [7]

$$A_{eff}(\alpha) = A_0 + A_1\alpha_{th} + A_2\alpha_{th}^2 \tag{4.105}$$

$$\tag{4.106}$$

4.9 Humidifier

This model manages the humidification of the inlet air mass flow into the cathode of the fuel cell. $\dot{m}_{w,inj}$ in Equation 4.5 is governed by the humidifier model in order to raise the water content when desired. The implementation of the humidifier is actualized by a PI-controller, having ϕ_{ca} as the measurement signal, the desired value of ϕ_{ca}, $\phi_{ca,ref}$, as the reference signal, and $\dot{m}_{w,inj}$ as the control signal. Since the model itself does not include any dynamics, the response of $\dot{m}_{w,inj}$ can be made arbitrarily quick.

4.10 Control Volumes

The model for the temperature inside the control volume is based on mass and energy conservation. The mass balance gives that the time derivative for the mass

in the receiver is equal to

$$\frac{dm_R(t)}{dt} = \dot{m}_{in} - \dot{m}_{out} \tag{4.107}$$

The temperature can then be derived from the energy balance, where the internal energy is

$$E_r = m_R c_v T_R \tag{4.108}$$

and the time derivative

$$\frac{dE(t)}{dt} = \frac{dm_r(t)}{dt} c_v T_R + \frac{dT_r}{dt} c_v m_r = \dot{H}_{in} + \dot{H}_{out} + q_{in} \tag{4.109}$$

With Equation 4.109 and the fact that the enthalpy can be described as $\dot{H} = \dot{m} c_p T$, the derivative of temperature T_R can be solved to be

$$\frac{dT_R(t)}{dt} = \frac{1}{m_r c_v} \left(\dot{m}_{in} c_p T_{us} - \dot{m}_{out} c_p T_{ds} + q_{in} - \frac{dm_R(t)}{dt} c_v T_R \right) \tag{4.110}$$

where $c_v = \frac{R}{k-1}$. k is the ratio of the specific heat. The pressure is then determined by the ideal gas law

$$pV = nRT_R \tag{4.111}$$

which can be rewritten as

$$p = \frac{m_R R T_R}{VM} = \frac{m_R R_{specific} T_R}{V} \tag{4.112}$$

where V is the volume, T_R the temperature, m the mass, and $R_{specific}$ the specific gas constant.

5

Parameter Estimation and Validation

In this chapter, the method and result for the parameter estimation will be presented. In general, public data was hard to find on fuel cells, hence estimations were done on the data that could be found.

5.1 Mass Flow Estimation in Fuel Cell

To estimate how the mass flow in fuel cell depends on the pressure and current all these signals need to be measured or calculated. The data for the estimation in this thesis was taken from [18]. The parameter was estimated according to a least-square estimation and the result can be seen in Table 5.1. The estimation fit the data well in almost all the regions which can be seen in Figure 5.1.

Table 5.1: *Parameter estimation*

Parameter	Value
K	$1.114 \cdot 10^{-7}$

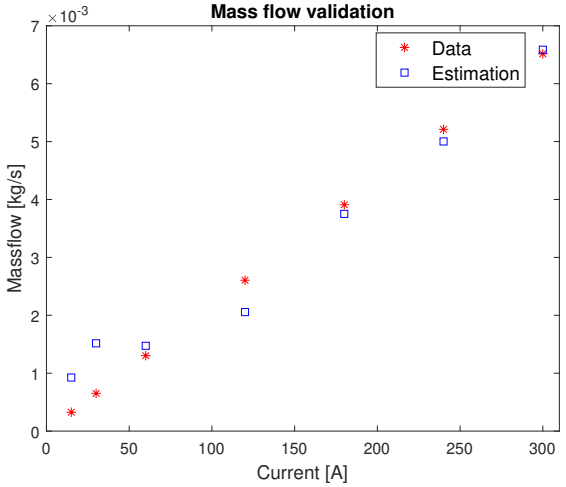

Figure 5.1: *Mass flow estimation validation. The red stars are real data and the blue squares are the estimations based on the data. The estimation fit the data well in general, with some deviation at low currents.*

5.2 Throttle Effective Area Estimation

The effective area is estimated according to Equation (4.105). For this thesis, the throttle data was taken from a combustion engine test, hence it may be oversized for the system but the method is the same for a smaller throttle. The compressor data was also sorted, by removing values where Π is close to one because the model is not well defined around this value. The estimation was done by a least-square method and is presented in Table 5.2. The validation of the estimation in Figure 5.2 shows a good estimation across all the measured data.

Table 5.2: *Effective area validation*

Parameter	Value
A_0	$1.2084 \cdot 10^{-5}$
A_1	0.00016335
A_2	0.0026013

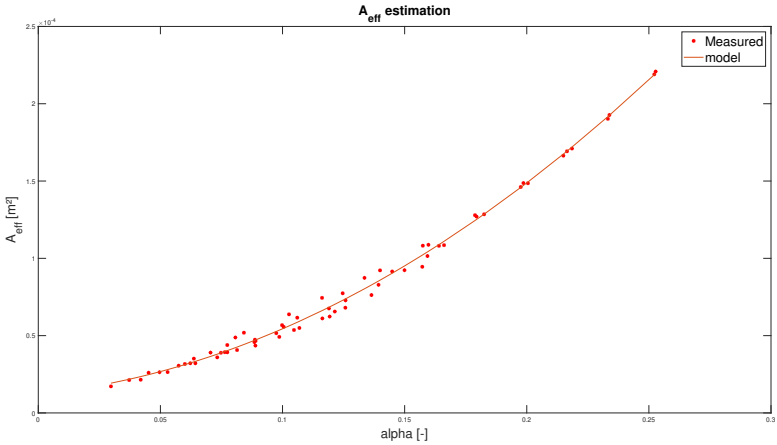

Figure 5.2: *Effective area estimation. The red stars are measured data while the orange line represents the estimation.*

5.3 Compressor Estimation

The tool to estimate the parameter needed for Equation (4.94) is provided by [20–22]. The estimation for our thesis was done on a turbo compressor for an internal combustion engine.

Table 5.3: *Estimated parameters for the compressor that was used in this thesis*

Paramteter	Value
$C_{\dot{m}ch,1}$	0.800658425052176
$C_{\dot{m}ch,2}$	0.234449958757705
$C_{\dot{m}ch,3}$	2.63982318981609
$C_{\dot{m}ch,4}$	1.33924842211382
$C_{\Pi ch,1}$	0.0830571419272955
$C_{\Pi ch,2}$	0.598066646900060
$C_{\Pi ch,3}$	3.99336167376410
$C_{\dot{m}zs,1}$	0.784661686468195
$C_{\dot{m}zs,2}$	2.64671304270013
$C_{\Pi zs,1}$	0.976728373102719
$C_{\Pi zs,2}$	2.20478848028108
$C_{cur,1}$	2.23855302183528
$C_{cur,2}$	2.33475537115463
$C_{cur,3}$	6.60989382532647

5.4 Efficiency Estimation of Traction Motor

The efficiency for a motor can in most cases, be estimated to a polynomial function. The polynomial function is also often a Taylor series, where the degree is specified by the user. The polynomial function can also be custom depending on what kind of behavior is of interest or what physics dependencies that are known.

For the traction motor, it is known that the power required by the engine is proportional to the power in. Hence the estimation should have a term eP_{in}. There should also exist a static loss in most motors hence a term C_1. For the rest of the terms, a Taylor series is used and then validated against measured data. For the test data, a degree according to Equation (5.1) fitted the data well without being too complex, as shown in Figure 5.3. The estimated variable can be seen in Table 5.4

$$P_{TM,est}(T_{tm}, \omega_{tm}) = eT_{tm}\omega_{tm} + c_1 + c_2\omega_{tm} + c_3\omega_{tm}^2 \tag{5.1}$$

Table 5.4: *Traction motor losses estimation*

Parameter	Value
C_1	905.3796
C_2	-53.7358
C_3	0.1681
e	1.2215

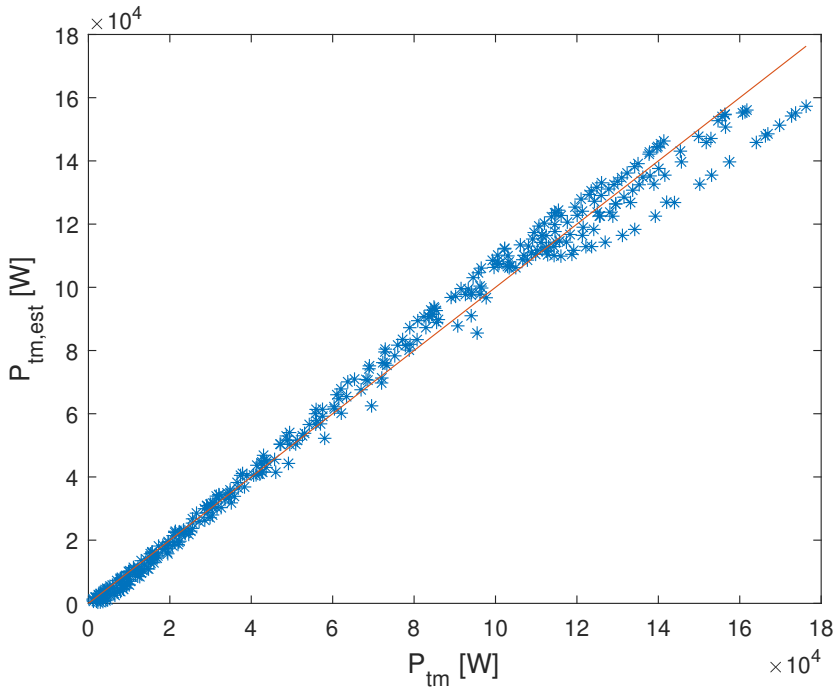

Figure 5.3: *Traction motor estimation. Estimated power on the y axis and power from data on the x axis. The red line has a slope of 1, which symbolises a perfect estimation.*

6
Model Validation

Many of the models are missing good validation data, hence a large part of the validation is performed by examining the results by comparing towards theory.

6.1 Fuel Cell

The fuel cell is divided into the same subcategories as before. While some models might be considered trivial, it may still be meaningful to validate that the results are still reasonable with all the dynamics that are implemented in this model.

6.1.1 Mass Flows and Humidity

Figure 6.1 shows the dynamics that follows from the current being dependent on the fuel cell reaction, and thereby the mass flows of reactants. At the start of the simulation, the current reference is stepped from 0 to 50 A, corresponding to a current density of 0.179 A/cm^2. At 500 s, a step is made to 100 A, corresponding to a current density of 0.357 A/cm^2. At 1000 s, another step is made to 150 A, corresponding to a current density of 0.536 A/cm^2. Figure 6.2 shows the mass flow water balance inside the cathode. A water content in the ambient air of 8 g/kg is assumed. Figure 6.3 shows the mass flow water balance in the anode, assuming no humidity in the stored fuel. Figure 6.4 shows how the relative humidity is affected by the fuel cell operating temperature, while the current density is held constant at 0.357 A/cm^2. Initially, the fuel cell temperature is 70°C. At 500 s, the reference temperature is stepped to 80°C, and at 1000 s another step is made to 90°C. It becomes apparent that higher temperature leads to drying. In summary, all these characteristics agree with the theory.

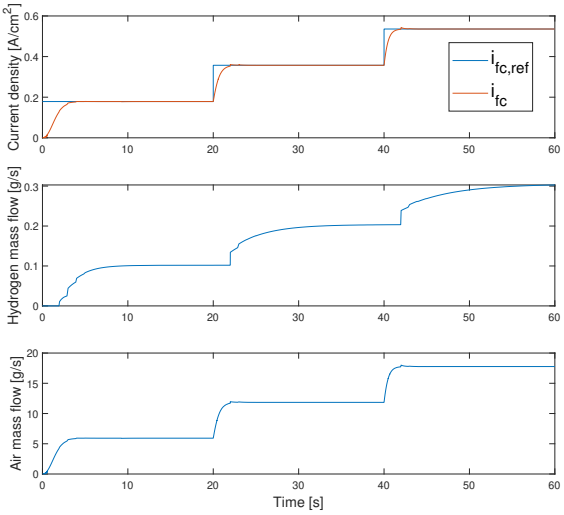

Figure 6.1: *The actual current delivered by the fuel cell is a function of the mass flows of the reactants. All modeled dynamics are included, and control reference parameters set according to Table 6.1. N = 300.*

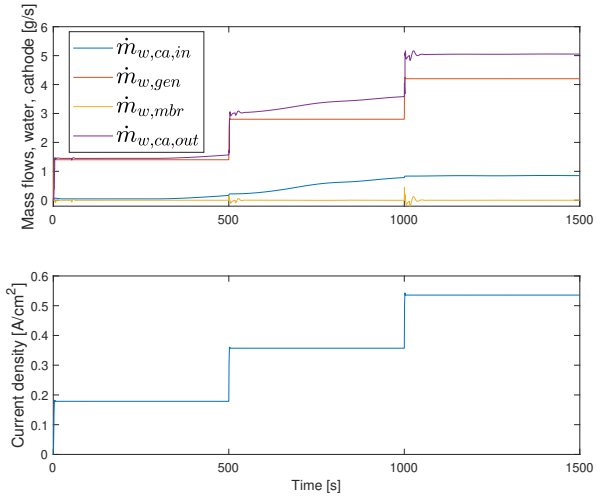

Figure 6.2: *Mass flow balance of water in the cathode. N_2-purging is disabled, so as not to interfere with the water mass flows. All other modeled dynamics are included, and control reference parameters set according to Table 6.1. N = 300.*

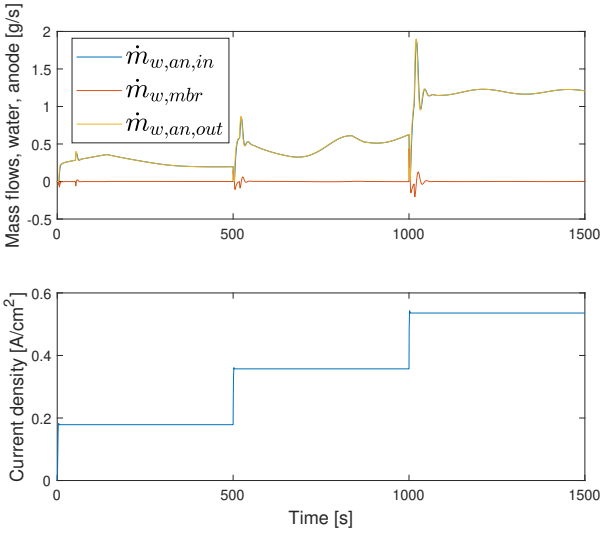

Figure 6.3: *Mass flow balance of water in the anode, under the assumption of no water contained in the fuel from the fuel tank. N_2-purging is disabled, so as not to interfere with the water mass flows. All other modeled dynamics are included, and control reference parameters set according to Table 6.1. N = 300.*

Parameter	Value
$T_{fc,ref}$	80[°C]
$\lambda_{a,ref}$	2[−]
$\lambda_{h,ref}$	1.3[−]
$p_{an,ref}$	$p_{ca} + 0.2[bar]$
$\phi_{ca,ref}$	0.85[−]

Table 6.1: *Control reference parameters used in the simulations in figures 6.1-6.4 and 6.7.*

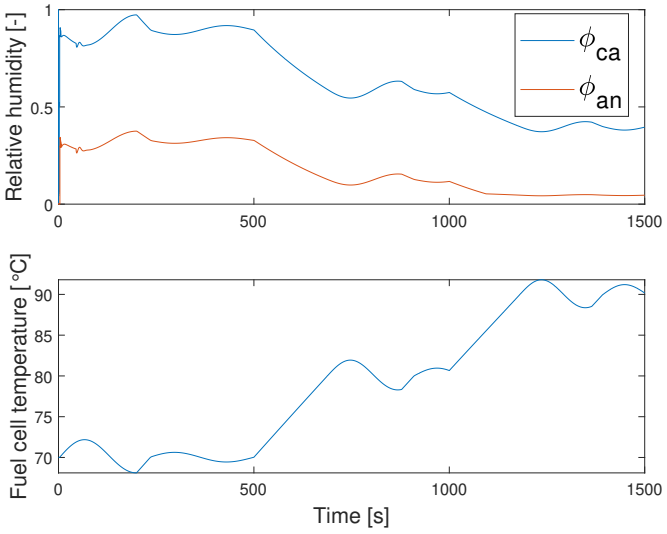

Figure 6.4: *The relative humidity affected by fuel cell operating temperature, as steps in $T_{fc,ref}$ are made. N_2-purging is disabled, and humidifier is disabled too. All other are dynamics included, and control reference parameters are set according to Table 6.1.*

6.1.2 Cell Voltage and the Polarization Curve

The polarization curve in Figure 6.5 clarifies the dependency on the operating pressure. The cathode pressure is set constant during simulation, according to the figure. The current is ramped, and all other variables affecting the voltage are set constant. Figure 6.6 shows the dependency of the voltage on membrane water content, and a higher humidity is favorable. The dependency on pressure, and membrane water content as well, agree with what is found in [27]. Figure 6.7 shows the polarization curve while all dynamics are included, except for $\lambda_a = 1.1$. The reason for the lower setting is because of limitations in the operation of the compressor. The current density surpasses the practical operating point, in order to display a larger part of the polarization curve. The polarization curve maintains its characteristic look.

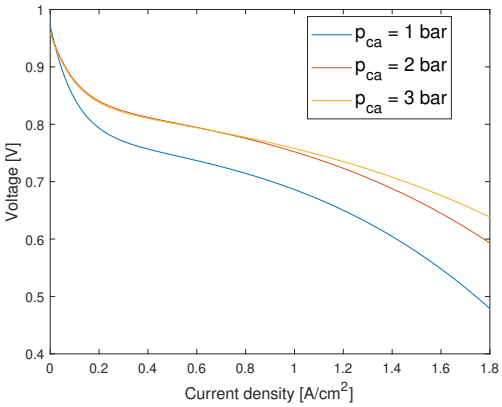

Figure 6.5: *Polarization curve showing dependency on operating pressure, while* $T_{fc} = 80°\text{C}$, $p_{an} = p_{ca} + 0.2bar$, $\lambda_m = 14$.

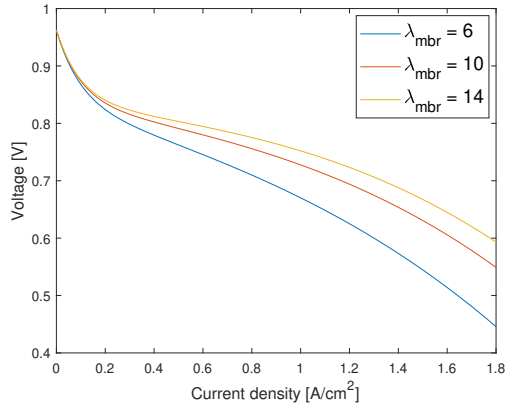

Figure 6.6: *Polarization curve showing the dependency on membrane water content, while $T_{fc} = 80°C$, $p_{ca} = 2bar$, $p_{an} = 2.2bar$. $\lambda_m = 14$ corresponds to a fully humidified membrane.*

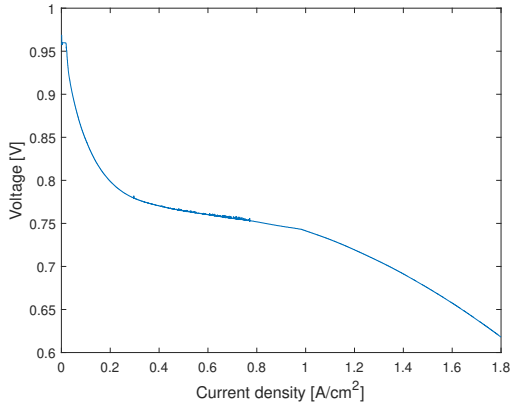

Figure 6.7: *Polarization curve with all modeled dynamics included. Control reference parameters set according to Table 6.1, except for $\lambda_a = 1.1$.*

6.1.3 Thermodynamics

The difference $(U_{id} - U_{fc})$ in Equation (4.42) is a measure of the voltage losses. The higher the losses, the higher the heat generation. Also, the higher the current, the higher the heat generation should be. Figure 6.8 shows how the modeled heat generation varies with the voltage losses and the current. The temperature model is otherwise based on the work in [18], and will not be validated in this thesis. Figure 6.9 shows the fuel cell efficiency while ramping the current. The behavior is reasonable. Note that $\lambda_a = 1.1$, as explained why in the previous section.

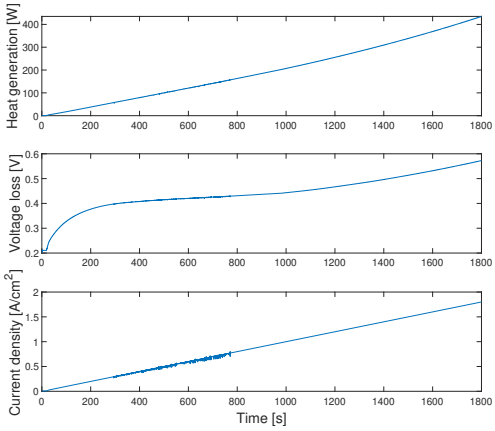

Figure 6.8: *The fuel cell heat generation, for a single cell, showing dependency on voltage losses and current density. All modeled dynamics are included, except for* $\lambda_a = 1.1$*, and control reference parameters are set according to Table 6.1.*

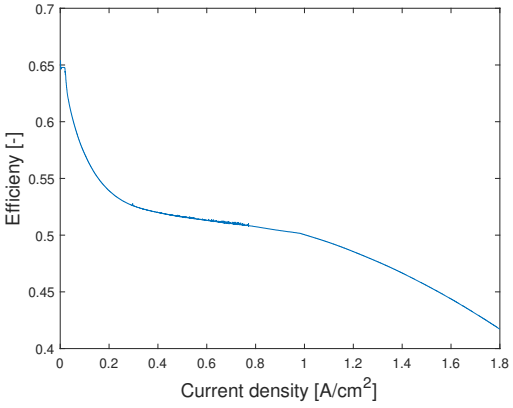

Figure 6.9: *The fuel cell efficiency, decreasing as the voltage is dropping and the current is increasing. All modeled dynamics are included, except for* $\lambda_a = 1.1$*, and control reference parameters are set according to Table 6.1.*

6.1.4 Purge Valve

The purge valve validation should purge the system when the nitrogen concentration reaches 25 % which can be seen in Figure 6.10. The purge works by clearing out all the pressure in the system which can be seen in the bottom two plots in Figure 6.10. The purge valve is open for 1s and then closed. When the purge

valve is then closed, both the concentration of nitrogen and the pressure should start to increase again, which can be seen in the lower two plots in Figure 6.10.

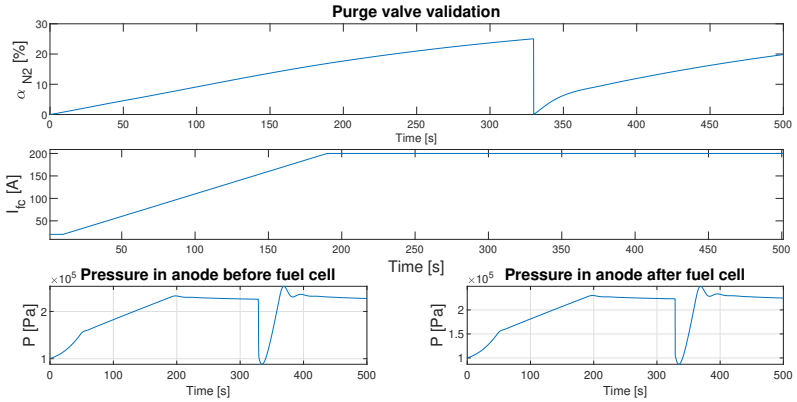

Figure 6.10: *Purge valve validation. The top plot is the nitrogen concentration, followed by a current plot. The last two plots is the pressure before and after the fuel cell*

6.2 Complementary Energy Storage

The battery and the supercapacitor is validated in this chapter.

6.2.1 Battery

Figure 6.11 shows the overall behavior of the battery model. Steps in the input signal, I_b, displays dynamic responses of the other signals. It is clear that a higher c-rate leads to lower efficiency, as well as lower battery voltage, in the modeled output. The same magnitude of discharging and charging has occurred during this simulation. The lower SoC at the end of the simulation is a sign of the model taking into account energy being lost to heat, a consequence of the efficiency. The heat generated is proportional to the load. in Figure 6.12, the input to the model is held constant over the course of the simulation. The output of the model makes it clear that the voltage, and the efficiency, are dependent on the SoC. Any variation in the heat generation with respect to time is not visible, and this is due to the fact that as the efficiency gets lower, so does the power output, with the same dependence. In summary, the battery model has a reasonable and expected behavior.

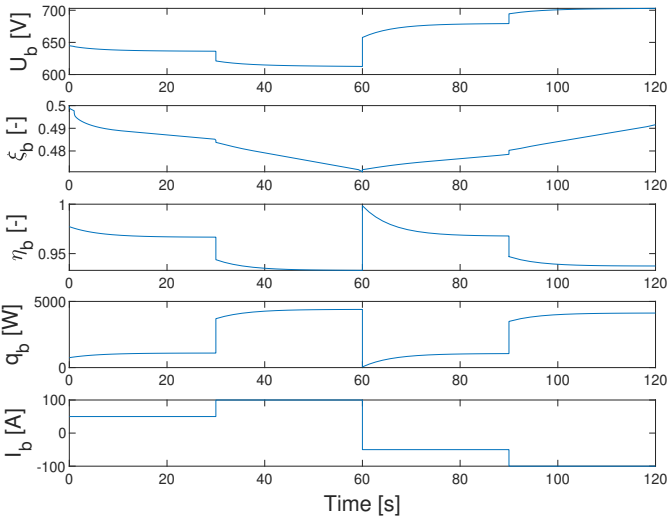

Figure 6.11: *The step response of the battery model exhibits dynamic behavior.*

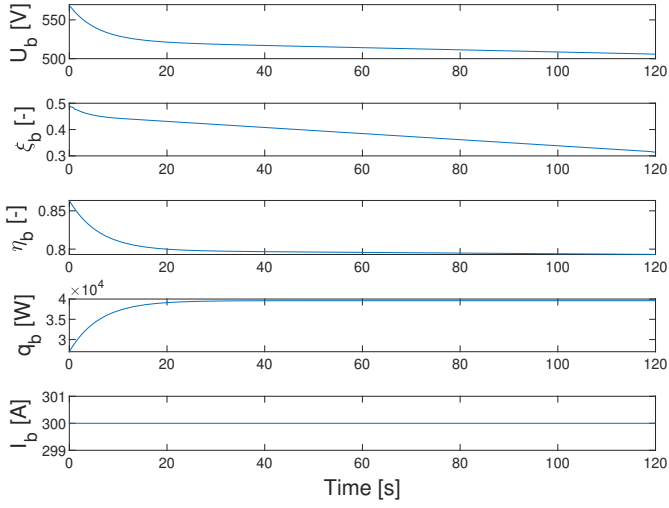

Figure 6.12: *Output of the battery model under constant load, making it easier to discern the static dependency of the signals.*

6.2.2 Supercapacitor

In [4], voltage levels are validated with cycles of charging and discharging. Figure 6.13 confirms that the modeled SoC is quadratically dependent on the voltage, as according to Equation (4.63). It is also possible to make out the self-discharge, during the time while no current is present. Equation (4.64) implies that the higher the charge of the supercapacitor, the less dependent the efficiency is on the current. This agrees well with the simulated charge/discharge test in Figure 6.14. The heat generation varies little with respect to efficiency. This is due to the fact that the charge level affects both the efficiency and the power delivery, where higher charge simultaneously leads to higher efficiency and higher power, and vice versa.

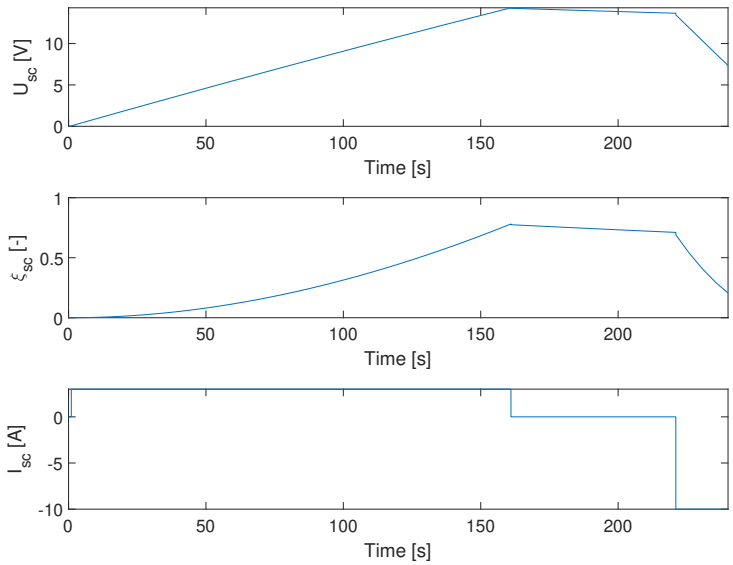

Figure 6.13: *SoC showing quadratic dependence on voltage.*

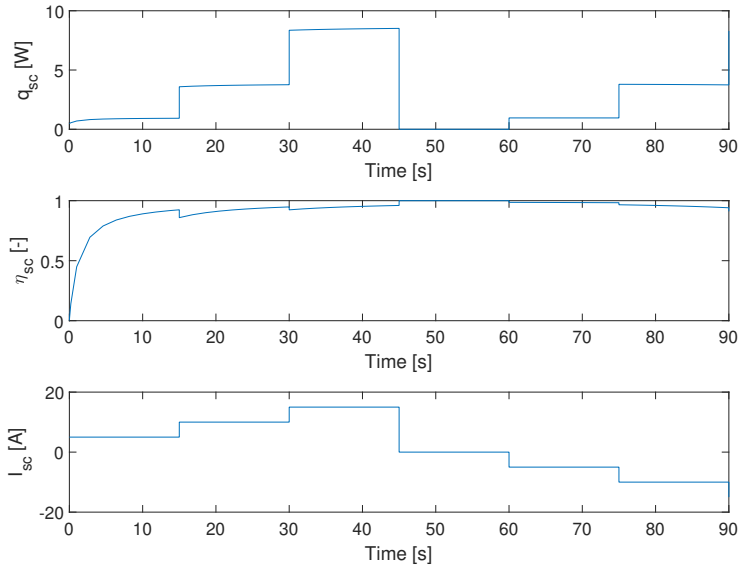

Figure 6.14: *Behavior of efficiency and heat generation of the supercapacitor.*

6.3 Traction Motor

The traction motor should need more power from the system when driving $P_{out} > P_{in}$ since the system needs to compensate for the losses. The reverse should happen when the traction motor is regenerative braking $P_{out} < P_{in}$. Both these behaviors can be seen in Figure 6.15. The losses are also estimated based on data and correlate well which can be seen in Figure 5.3, hence the model is valid.

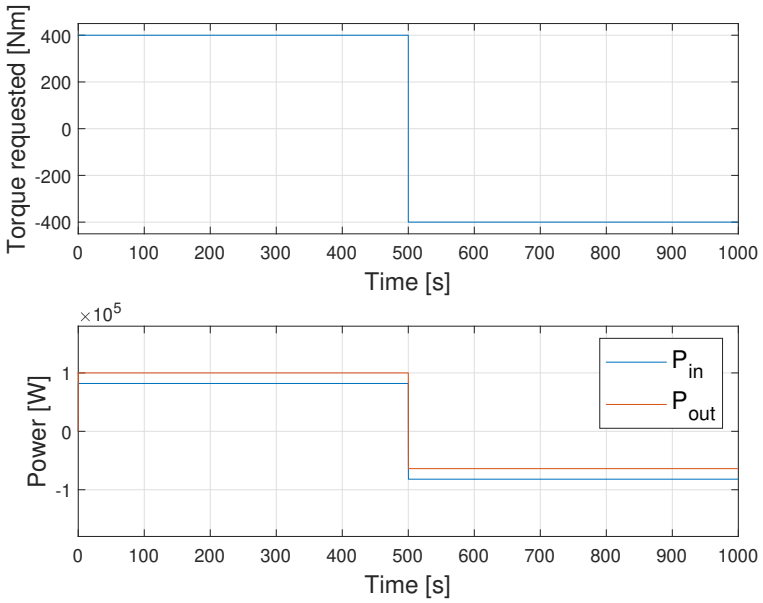

Figure 6.15: *Torque test of the electric motor*

6.4 Power Management

The converters between different current source are not validated since they only depend on a stationary efficiency. The DC to DC converter is validated below.

6.4.1 DC to DC

The DC to DC converter converts the input voltage to the output voltage by a variable D. This variable in turn affects the efficiency. Hence a decrease in the voltage difference between input and output should increase the efficiency. The efficiency should also affect the current the converter needs to be provided with. Both these behaviors can be seen in Figure 6.16

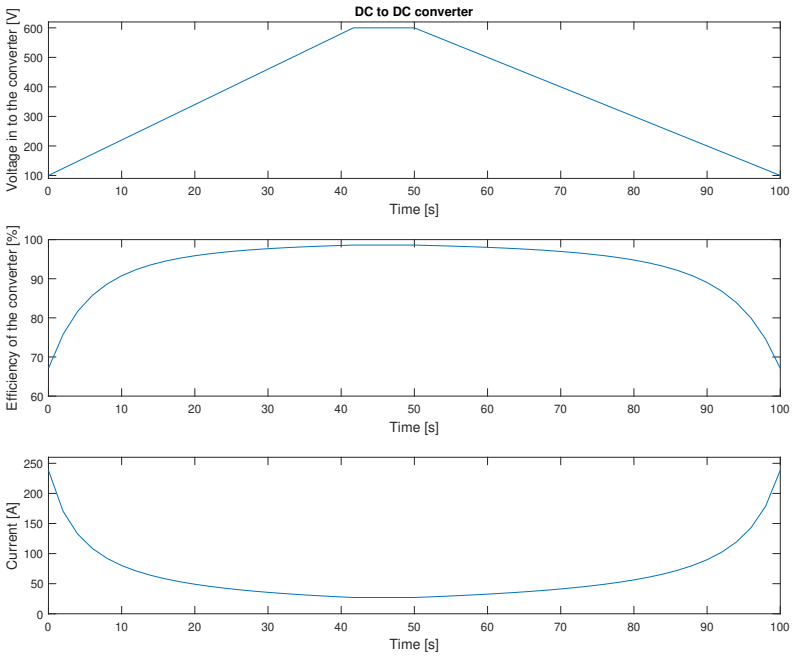

Figure 6.16: *Validation for the DC to DC converter. The voltage at the output of the converter is 700 V and the input voltage is given by the first plot. The power that the system needs to provide is 16kW in this simulation.*

6.5 Air Circuit Auxiliary Components

Validation for the compressor and throttle is presented below.

6.5.1 Compressor

The compressor in Simulink is modeled and validated in [20–22], hence a detailed validation is not included in this thesis.

6.5.2 Throttle

The throttle should limit the mass flow and build pressure before the throttle. A ramp in the throttle plate angle can be seen in Figure 6.17. This should increase the pressure before the throttle which can be seen in Figure 6.17. Since this behavior correlates well to theory and the effective area is estimated based on data, the throttle is validated. One can also note that the mass flow through the throttle oscillates when the pressure before the throttle is close to the pressure after the throttle, 1 bar. This correlates well to the theory of the model approach since

it is not well defined around a pressure ratio of 1. However this is not a problem for the whole fuel cell system since the pressure in the control volume is barely affected, which can be seen in Figure 6.17.

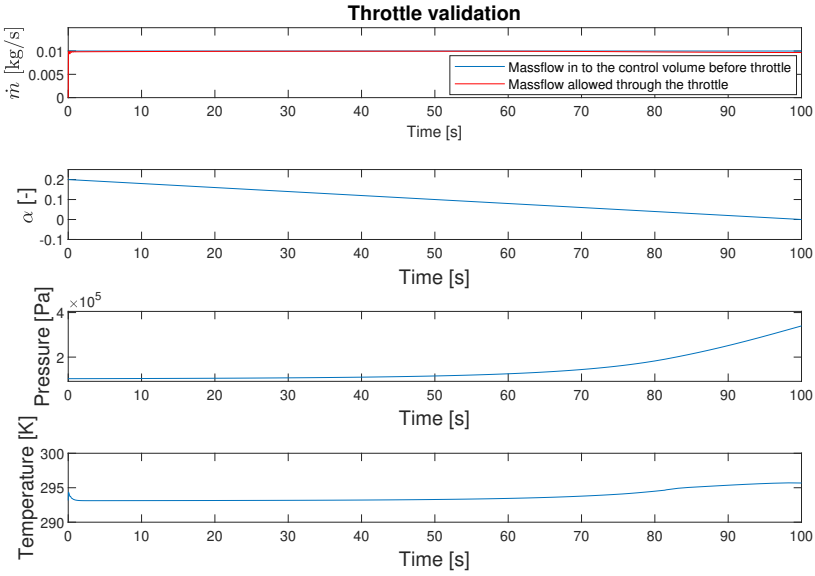

Figure 6.17: *Throttle system test. The first plot shows the mass flows, while the second shows the plate angle. The last two plots shows the temperature and pressure in the control volume before the throttle*

6.6 Cooling Circuit Auxiliary Components

The cooling system validation is presented in this section.

6.6.1 Radiator with fan

The radiator should cool the system differently depending on the speed and the temperature of both the air and the coolant.. The cooling effect should increase with the coolant speed or the air speed. This behavior can be seen in Figure 6.18 and 6.19. The system should also only turn on the fan when the temperature reaches a certain threshold, which in Figure 6.18 to 6.20 is 2 kelvin above the reference temperature. The fan does this in all tests which proves that the regulator for the fan works. The fan should also be able to cool the system when the vehicle speed is zero which is the case in 6.20. The fan in Figure 6.18 to 6.20 is a assumed to be able to supply a flow of 5kg/s at 80 W.

6.6.2 Bypass Valve and Pump Validation

The bypass valve redirects the flow in the system with the variable K. This variable K is in return controlled by a regulator that regulates the temperature. The bypass valve should direct the coolant to the radiator if the temperature is too high and bypass the radiator if it is too cold. This behavior can be seen in Figure 6.18 and 6.19 hence the model is valid.

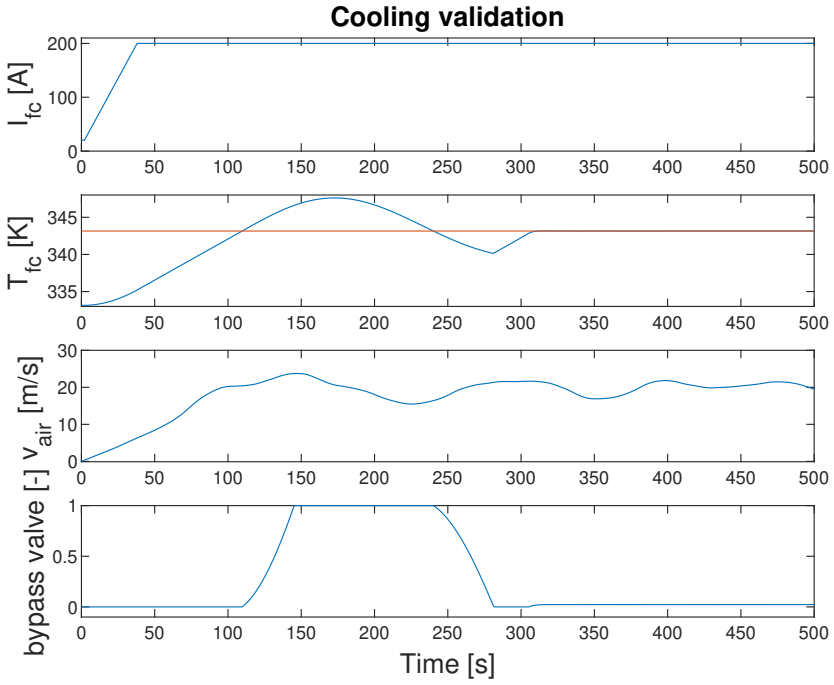

Figure 6.18: *Cooling test with a ramp in current as input, T_{amb} is 20 degree Celsius. The first plot shows the current while the second shows the temperature in the stack. The third plot shows the speed of the air while the fourth plot shows the bypass valve position.*

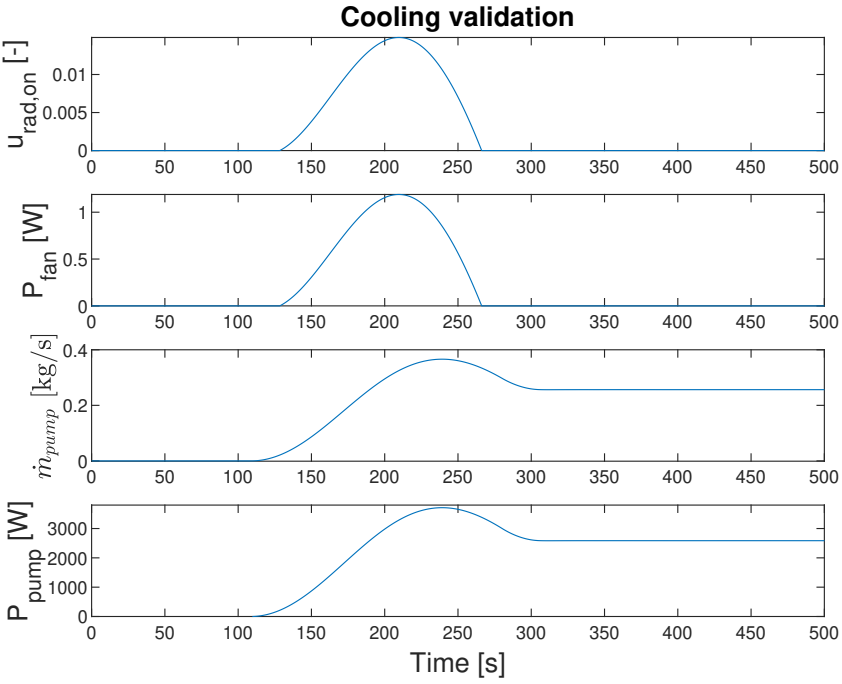

Figure 6.19: *Cooling test with a ramp in current as input, T_{amb} is 20 degree Celsius. The regulator for the fan regulates between 1 and zero, where 1 stands for max flow*

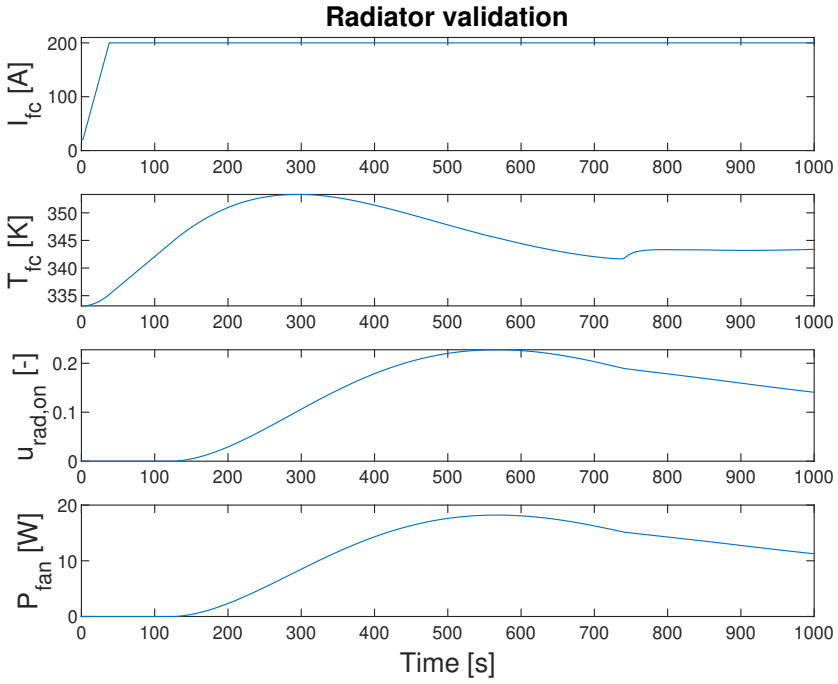

Figure 6.20: *Cooling test with a ramp in current as input, T_{amb} is 20 degree Celsius. The speed is set to zero in this simulation to see if the fan can cool the system.*

6.7 Control Volumes

The control volume pressure depends on the mass flow in and out, as well as the temperature in and out. Hence when the mass flow in is larger than the mass flow out, the system should build pressure and when the mass flow out is bigger than the mass flow in the pressure should decrease. This behavior can be seen in Figure 6.21, where the temperature is constant, and no heat transfer to the environment. The mass flow is ramped according to the first plot in 6.21.

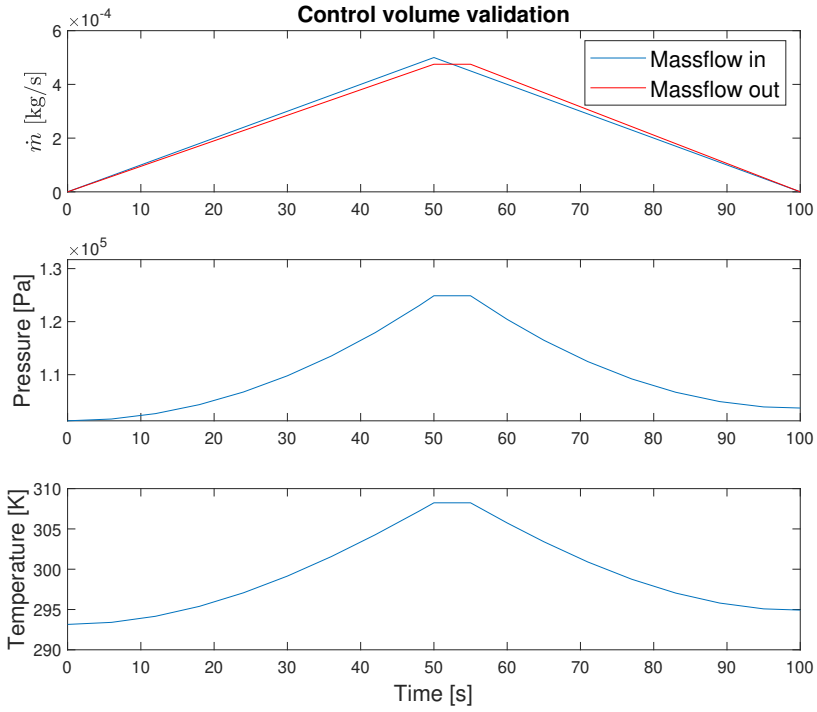

Figure 6.21: *Control volume test. Where the first plot shows the mass flows. The second shows how the pressure varies. The third shows the temperature inside the control volume.*

7

Simulations

7.1 Ramp Simulation

Firstly, in Figure 7.1, the performance of the fuel cell stack is displayed, in regards to power delivery and efficiency with respect to the current. Note that, in order to perform this ramp test, the reference value for λ_a is reduced to 1. This needs to be done due to the limits in the mass flow generated by the compressor. This is normally not a concern, since the current density in the ramp test far surpasses what is suitable for usable operating points. It is simply to illustrate the behavior of the fuel cell. The decreasing power at high current densities is mainly due to the concentration polarization.

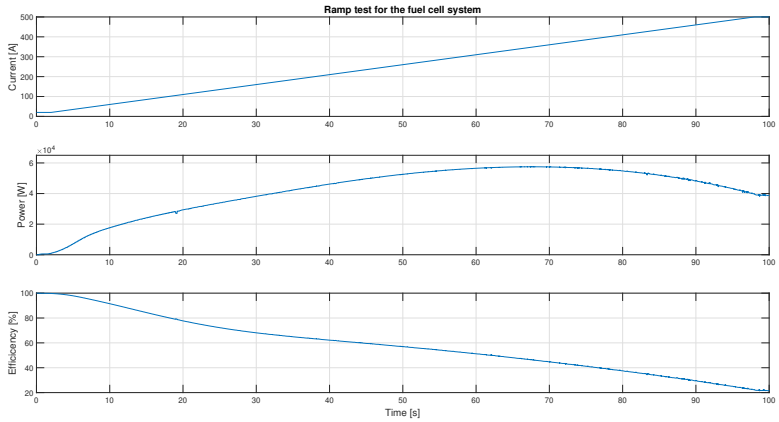

Figure 7.1: *Ramp test of the current for the fuel cell system*

7.2 Drive Cycle Simulation

The results presented in this section shows the signals for the first 1000 seconds of the "Södertälje-Norrköping" cycle. This is a drive cycle taken from [8], and contains a road profile. The component parameters used are presented in appendix A, along with a simulation of the complete cycle. The simulation is done in truckbenchmark from [8], where the internal combustion engine is replaced by an electric powertrain consisting of a fuel cell stack and a battery. The signals chosen to be displayed are the most crucial signals for the performance of the system.

Figure 7.2 clarifies the operation of the power management, distributing the supplied current between the fuel cell stack and the battery. The operation of the fuel cell is limited between two operating points, and the battery SoC is controlled to be kept around 0.5 by the power management. See Figure 7.3 for the fuel cell efficiency during this operation, and Figure 7.4 for the battery SoC.

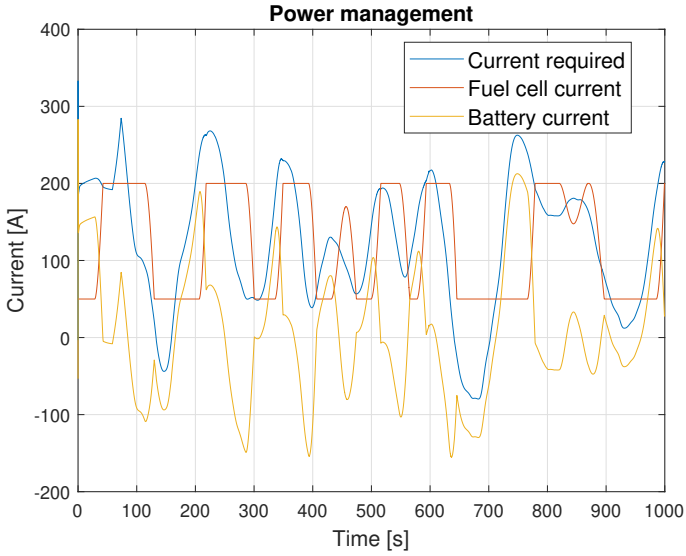

Figure 7.2: *Power management signal for the first 1000 seconds of the "Södertälje-Norrköping" cycle*

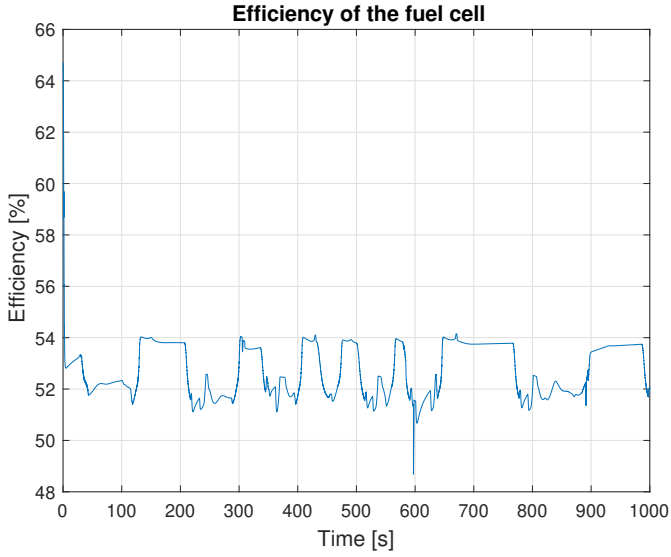

Figure 7.3: *The efficiency of the fuel cell for the first 1000 seconds of the "Södertälje-Norrköping" cycle*

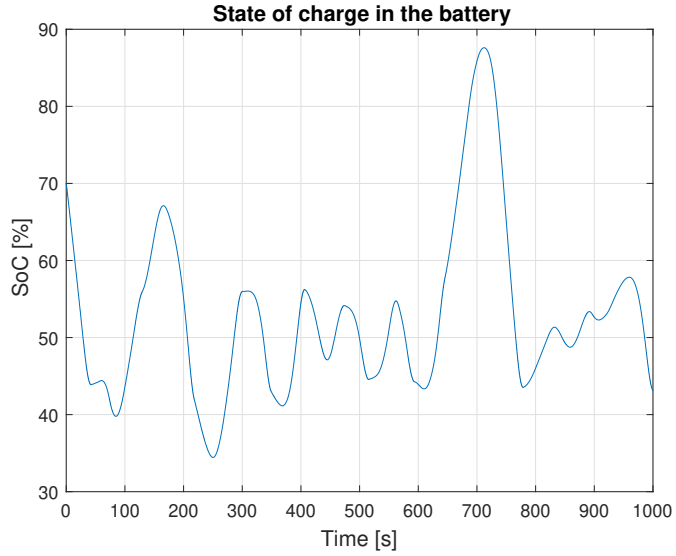

Figure 7.4: *The state of charge for the battery for the first 1000 seconds of the "Södertälje-Norrköping" cycle*

The temperature of the fuel cell stack is seen in Figure 7.5. The cooling system manages to keep the temperature close to the reference value of 343 K, or 70°C.

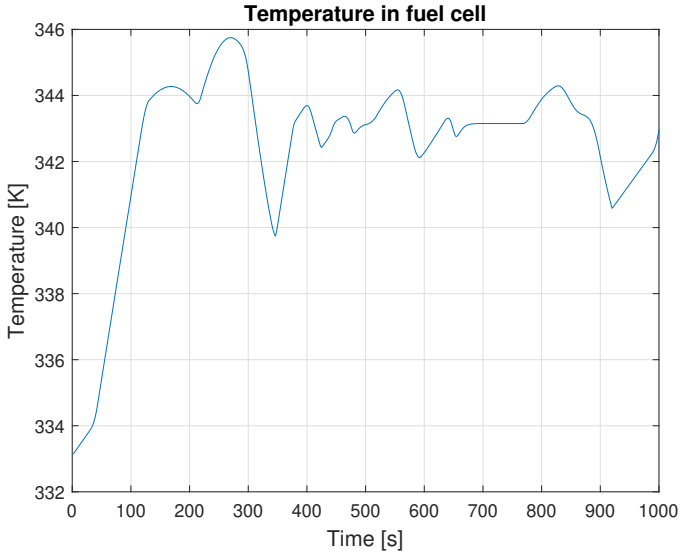

Figure 7.5: *The temperature inside the fuel cell for the first 1000 seconds of the "Södertälje-Norrköping" cycle*

Figure 7.6 shows the pressure difference over the membrane, between cathode and anode. Note that the largest difference, occurring at around 600 s, is a consequence of the N_2-purging.

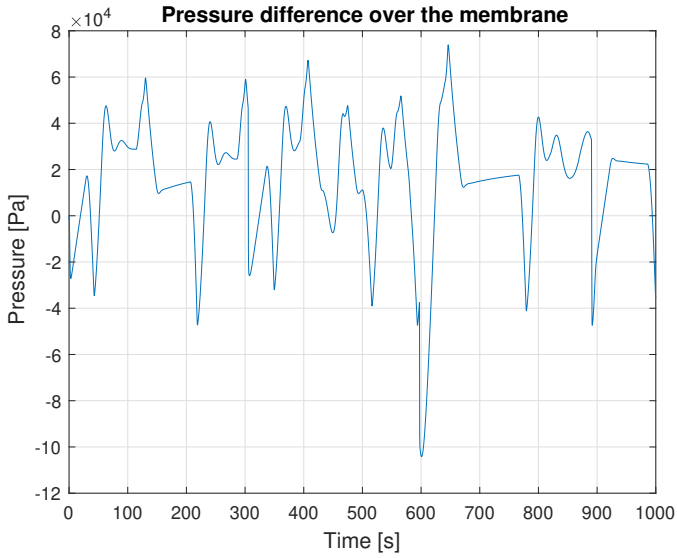

Figure 7.6: *The pressure difference over the membrane. A positive value means the anode has higher pressure, and vice versa. The simulation is the first 1000 seconds for the "Södertälje-Norrköping"*

The humidity levels during the simulation are seen in Figure 7.7. Note that the levels between the anode and cathode are correlated via the membrane water flux.

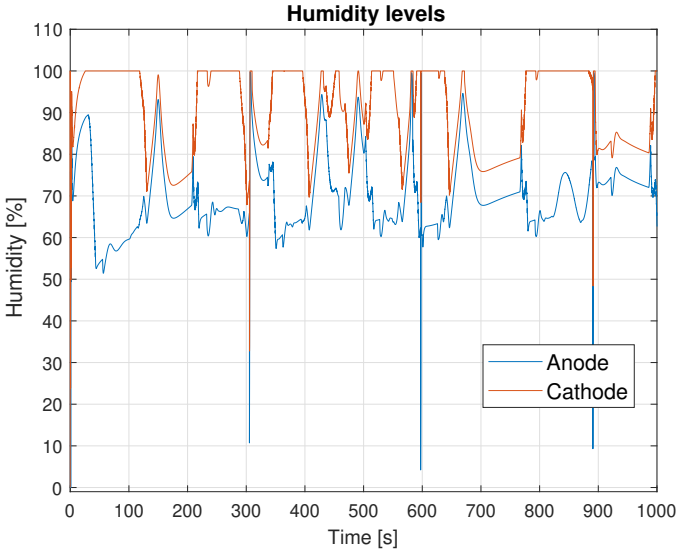

Figure 7.7: *The Humidity levels for the cathode and anode during the first 1000 seconds of "Södertälje-Norrköping"*

8 Discussion

In this chapter a discussion about the results and method is presented, followed by a discussion about the work in a broader perspective.

8.1 Results

The results in Figure 7.1 to 7.7, and the validation in chapter 6, proves that a component-based fuel cell system has been achieved with good performance. However, there are some limitations and behaviors that are of interest to be discussed.

One of these interesting behaviors is how the efficiency and power correlate to how much current the fuel cell supplies. With increasing current, the fuel cell efficiency decreases. As can be seen in Figure 7.1, the power increases with increasing current to a certain amount, reaching a maximum value. While the fuel cell still can handle higher currents at this point, the output power will decrease. Hence, there is no gain in increasing the current further. Both these behaviors correlate well to theory around the polarization curve for the system which can be seen in Figure 6.7. This behavior is of extra interest since it proves the importance of decent power management when the fuel cell is used in a hybrid configuration. It also proves how important the sizing of the stack is.

Another aspect of interest is the pressure difference over the membrane. With a higher pressure difference over the membrane, the risk of damaging the membrane increases. As an industrial standard the pressure difference should not exceed 0.5-1bar [18]. As can be seen in Figure 7.6, the system sometimes exceeds these bounds. The highest pressure differences is often because of the purge valve releasing the pressure of the anode, while the cathode pressure remains high.

This behavior could be minimized with a better control strategy for purging.

In Figure 7.3, it can be seen that the efficiency of the fuel cell varies between about 48-54 % during the drive cycle. [10, p. 206] states that the practical efficiency of a PEMFC is in the range of 50-60 %, and the result is therefore considered reasonable. Since the fuel cell efficiency is dependent on several things, the result could be slightly different by adjusting the operating parameters. Simply shifting the limits of allowed operating points would have a considerable impact on the efficiency.

The membrane is also sensitive to the humidity levels inside the fuel cell, and should be kept not too high and not too low [28]. The humidity levels of the system model, during simulation, are at some operating points hard to control, which can be seen in Figure 7.7. This could probably be improved slightly with tuning of regulators, but keeping desired humidity levels seems to be a challenge also for actual fuel cells. Another factor that affects the humidity is that the cathode pressure regulator is not optimal since it only regulates the throttle plate angle. A better strategy would be to regulate both the compressor mass flow and throttle plate angle.

The power management is also a system that affects many other systems by changing the operating point and hence can be of interest to further analyse. As can be seen in Figure 7.2, the power management varies the operating point of the fuel cell, while keeping it between an upper and a lower limit. At the same time, it manages the battery SoC, with a reference value of 50%. This power management works well, but has its shortcomings. It is not affected by the SoC exceeding the limits, meaning that sizing the powertrain components properly before simulation is needed for reasonable results. This will also affect how well the power management succeeds in keeping the battery SoC around the reference value. Figure 7.4 shows large variations in SoC. While the battery SoC does not exceed reasonable limits during this simulation, modifications of component parameters could impact the extent of the deviations.

8.2 Method

A significant issue for this thesis has been the choice of level of complexity for each subsystem and model. Generally speaking, every model is an imitation of reality with simplifications. The level of complexity might impact the simulation results to a varying degree, depending on which model it concerns and the extent of simplification. The method has been to choose the level of complexity of each model by reasoning about how crucial the model should be for the system in full, and expand the complexity of less central models if time allows. Having a limited amount of time has often been the main reason for a lower level of complexity for several models. What effect the complexity of a particular model may have had is not really fully known. One could argue that another reason to sometimes consider a lower level of complexity is the impact on the simulation time that the level of complexity might have. However, this aspect has not been investigated

in this thesis. Further, systems represented by dynamic models often need to be controlled. Regarding the control strategies in this thesis, it has been kept on a fundamental level. Different versions of simple PID-controllers is implemented where a control system is needed, and not much care is involved with tuning these controllers. After all, the purpose of this thesis work is to model the powertrain system, and not to optimize the operation of it. Having that said, we believe we succeed in controlling the system with decent performance.

Regarding the FC, it itself is a rather complex subsystem, so the model of the FC resulting in high complexity is hard to avoid. Altough, since the modeling of the FC is the main focus of this thesis, a higher level of complexity for the associated models is considered appropriate and desirable. A dynamic model is often chosen over a QS model in this thesis, and several expansions have been made based on the work from several different sources, in order to increase the complexity and dynamic elements additionally. For other models, the method of implementation has been as described above, and we refer to chapter 4 for more details of each model.

The utilization of control volumes leads to the connection of one subsystem to another being standardized for the whole system. For the sake of simulation, this also leads to a straightforward way of avoiding algebraic loops, while adding dynamics and complexity at the same time. Besides, this is also a way of saving time during the implementation of models.

The lack of validation data could be considered a shortcoming of this thesis. The validation has mostly been about assessing the credibility of a simulation in relation to available theory, but ideally the simulation results would to a greater extent be compared with actual data.

8.3 The Work in a Broader Perspective

The system model developed in this thesis could help the world develop a more environmentally friendly transport industry. However, if the infrastructure of H_2 production does not improve, the positive gain to the environment will be less since e.g. around 95% of hydrogen right now is produced by natural gas in the USA [1].

9

Conclusions and Future Work

In this chapter, the thesis problem statements will be answered, and future work will be presented.

9.1 Conclusions

It has been determined which major subsystems make up the powertrain of the type of FCHEV regarded in this thesis. These are

- Fuel cell
- Purge valve, and fuel contamination
- Battery
- Supercapacitor
- Traction motor
- Power electronics
- Power management
- Radiator
- Bypass valve
- Compressor
- Throttle
- Humidifier

- Pumps (Cooling circuit, hydrogen circuit)

Not all subsystems listed does necessarily need to be modeled in order for the system to give reasonable results. For instance, the water trap has not been modeled. Instead, an assumption is made that all the excess water leaving the fuel cell can be removed. The same goes for the humidifier, where the approach is to simply implement it as a regulator. Although, the primary subsystems that make up the powertrain needs to be modeled. For auxiliary components, what subsystems that needs to be modeled is in some ways a matter of choice of complexity level. The meaning of the first part of the first question thus in a way converges with the second question. Regarding how the subsystems will connect and interact, this has been standardized in order to meet the objective of the model being component-based. The thermodynamic control volumes manages signals between subsystems for mass flow and pressure, and also takes into account temperature differences and external energy flows to or from the volume. Input signals are mass flow in & out, temperature in & out, and external energy flow, while the resulting pressure is the output signal. In terms of electrical power signals, all subsystems concerned are standardized to require current as input signal, and voltage as output signal. The power distribution, and interaction between associated models, is managed by the power management model.

With a higher level of model complexity, the aim is to obtain a simulation result closer to reality. This may mean that a model takes into account dynamic phenomena, but it can also mean the inclusion of other surrounding details of a system. In this thesis, the level of complexity for the models directly affecting the fuel cell performance is given higher priority than for other models. Especially the voltage model, since this is the output of main interest by the fuel cell. Also, the voltage behavior is rather complex in reality, and needs a rather high level of model complexity in order to yield reliability. The operating temperature has a significant impact on the performance and overall behavior of the fuel cell, which justifies aiming for a higher level of model complexity also for the models regarding heat generation, and temperature, of the fuel cell. However, in that case it is all the more favorable to also strive for a higher model complexity for the models concerning the cooling system as well. Since the humidity levels inside the fuel cell also plays a major role for its performance, this needs to be recreated in the model. The behavior of the water mass flows and humidity levels is quite intricate, which inevitably leads to a higher level of model complexity. In summary, the fuel cell requires a relatively high level of model complexity. For the other models, the reasoning that a more complex model in general gives higher accuracy, along with longer simulation time, applies. Exactly what consequences a certain extension of a model might have, varies. For many of the subsystems in this thesis a considerably high level of model complexity is applied, and the system does not need unreasonably long simulation times. On average, the complete hybrid system model during a drive cycle currently simulates about 67 times faster than real time. This simulation speed is measured with an Intel Core i7-6700HQ CPU running at 2.6 GHz with 8 GB ram running at 2133MHz.

All of the models are validated either against data, or against theory. Validation against data implies an assurance of reliability, while the validation against theory confirms a reasonable behavior along with values in the correct order of magnitude. Thus, the models correspond well to reality. See chapter 6 for details surrounding the validation of each submodel.

9.2 Future Work

Presented in this chapter are thoughts and suggestions about further development, and some possible extensions for the models.

9.2.1 Control strategy

All the regulators in this thesis are either a PI or PID regulator, which poses some problems with stability if not tuned correctly. The regulators also interferes with each other, as a consequence of cross correlation. Both these problem could be solved by a multi-variable regulator like Linear–quadratic regulator (LQ) or Model predictive control (MPC). With a strategy like MPC, constrains could be implemented and more.

9.2.2 Improve the power management

The power management in this thesis is a simple PI controller that regulates the SoC towards a specified constant value. This is not as suitable for the operation of the supercapacitor, since its behavior and area of use is different from the battery. The power management does not detect SoC-window either, which has limits that should not be exceeded. An idea to solve this problem is to use an advanced logic regulator with combinations of several if- and/or while-statements.

9.2.3 Benchmark the model

Most subsystem models are validated primarily without real data, which poses some questions about how well the whole system correlates to reality. How well the system model correlates to reality could be answered and corrected by a benchmark test done on a fuel cell system setup.

9.2.4 Battery capacity & C-rate

The battery capacity is actually a function of the applied current, while the nominal capacity is determined with constant-current discharge/charge tests. While determining the operating point and efficiency of the battery, it is common to consider a non-dimensional value called C-rate, which takes into account also the varying capacity, in addition to the current. C-rate is defined as

$$c(t) = \frac{I_b(t)}{I_0}, \quad I_0 = \frac{Q_0}{1hour} \tag{9.1}$$

where I_0 is the current that discharges the battery in one hour. Considering how Equation 4.51 depends on $I_b(t)$ and U_{oc} (and thus the SoC and C-rate), the C-rate is a more accurate way of representing the operating point of the battery. I.e., solely taking into account the battery current and nominal capacity is a simplification.

The efficiency is affected by this, hence why it would be of interest to implement in the model.

9.2.5 Liquid Water Formation and Flooding

While higher humidity levels of the PEM greatly improves the performance and longevity of a fuel cell, exceeding a relative humidity of 100% leads to flooding, and has a negative impact on performance. At this point, water is condensing into liquid phase, blocking the pathway of reactants through the membrane, along with other detrimental consequences. Modeling the negative effects of flooding would be an interesting extension for future work.

9.2.6 Water Tank, Water Separator and System Water Balance

In a real system, the humidifier during its operation picks up water stored in a tank. On the outlet stages of the fuel cell, a water separator may be used to collect water from the exhaust gases back to the tank. It is of great importance to have enough water for the humidifier to operate properly, and the modeling of the interaction between water tank, water separator and humidifier would provide additional useful information for the evaluation of the system. The storage capacity of a water tank could be an additional degree of freedom for component sizing, and the ability of a water separator could be investigated in detail. Specifically for the anode circuit, since the exhaust gases are recirculated, a water separator might also be utilized to extend the control ability of the humidity levels, and prevent flooding.

9.2.7 Component Mass

The total mass of a vehicle affects the fuel economy directly. For future work, the mass of each component could be included and added to the total mass. An idea is to take into account parameters such as specific energy, specific power, energy density and power density.

9.2.8 More Configurations

This thesis did not experiment with different system configurations. The fuel cell in a hybrid configuration with both the battery and supercapacitor could be of

interest. The sizing of the different components can also be experimented with.

9.2.9 Fuel Cell Inlet Temperature

This thesis does not consider the inlet temperatures of the gases. This will have a certain impact on the fuel cell. To further analyse this, the heat transfer from the control volumes also need to be researched, since it is now assumed to be zero.

Appendix

A

Full drive cycle simulation

Table A.1: *Fuel cell parameters that were used to simulate the results for a full cycle. Also applicable for chapter 7.*

Fuel cell parameters	Value
Coolant heat capacity, c_p_coolant [J/(kgK)]	$4.184 \cdot 10^{-3}$
Number of fuel cells in series, N [-]	300
Electro-osmotic drag coefficient, n_d [-]	0.65
Faraday's constant, F [C/mol]	96485.3383
Active area, A_fc [m^2]	$280 \cdot 10^{-4}$
Convective heat transfer coefficient, k_conv [$W/(m^2K)$]	25
Cell thickness, t_cell [m]	$4 \cdot 10^{-3}$
Thickness of assembly bipolar plates, t_bp [m]	$5 \cdot 10^{-5}$
Membrane thickness, t_mbr [m]	$183 \cdot 10^{-6}$
Diffusion coefficient, D_w [-]	$1.5 \cdot 10^{-7}$
Double-layer capacitance, C_dl [F]	5
Fuel cell mass density (net), rho_fc [kg/m^3]	1130
Specific heat capacity of fuel cell, average, c_fc [J/(kgK)]	8.2
Convective heat transfer coefficient, k_conv [$W/(m^2K)$]	10
Tuning parameter for activation polarization, a1 [-]	0.4
Tuning parameter for ohmic polarization, a2 [-]	3.5
Tuning parameter for concentration polarization, a3 [-]	2.5

Table A.2: *Radiator parameters that were used to simulate the results for a full cycle. Also applicable for chapter 7.*

Radiator parameters	Value
Efficiency, Motor that drives fan [-]	0.8
Efficiency, fan [-]	0.8
Height, radiator [m]	1
Width, radiator [m]	1
Pipe diameter [m]	$12.7 \cdot 10^{-3}$
Single loss factor [-]	0.29

Table A.3: *Battery parameters that where used in the simulation for the result in chapter 7.*

Battery parameters	Value
Open-circuit Voltage [V]	1000
Nominal cell voltage [V]	3.6
Charging Capacity [Ah]	30
Nominal cell capacity [Ah]	3
Double-layer Capacitance [F]	43.8
Maximum dis-/charging current [A]	600
Initial State of Charge [-]	0.7
Ohmic Resistance [Ohm]	$15 \cdot 10^{-3}$
Charge-transfer Resistance [Ohm]	$4 \cdot 10^{-3}$
Diffusion Resistance [Ohm]	$3 \cdot 10^{-3}$

Table A.4: *Other parameters used in the simulation.*

Other parameters	Value
Lambda air [-]	2
Lambda hydrogen [-]	1.3
Volume in the control volumes $[m^3]$	$3 \cdot 10^{-3}$
Gas constant $[J/kgK]$	286
Ratio of specific heat [-]	1.35

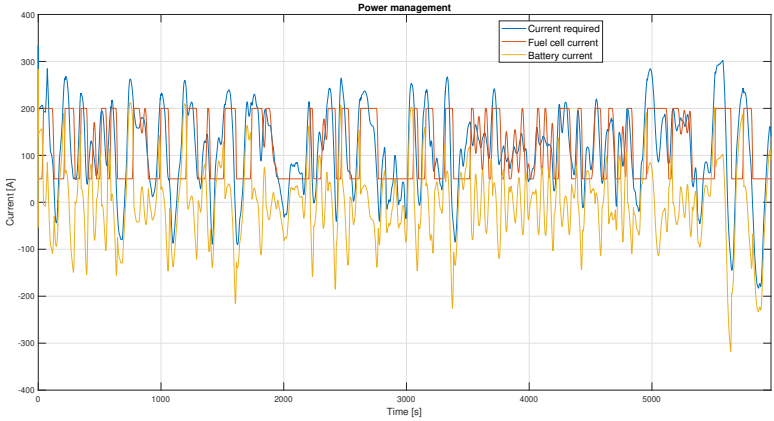

Figure A.1: *Power management between the fuel cell and the battery.*

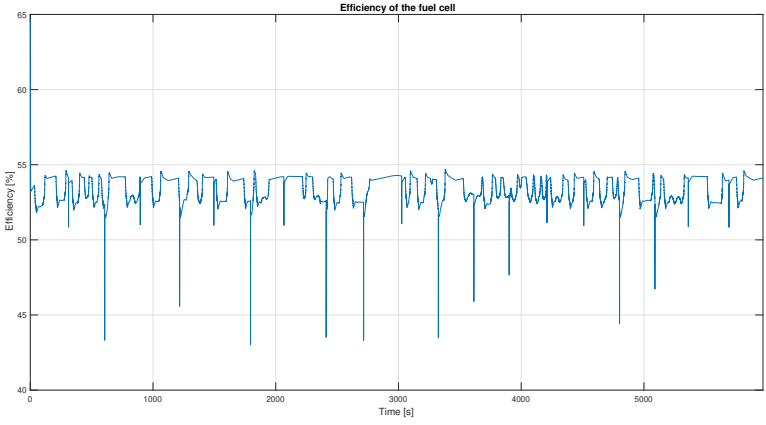

Figure A.2: *Fuel cell efficiency.*

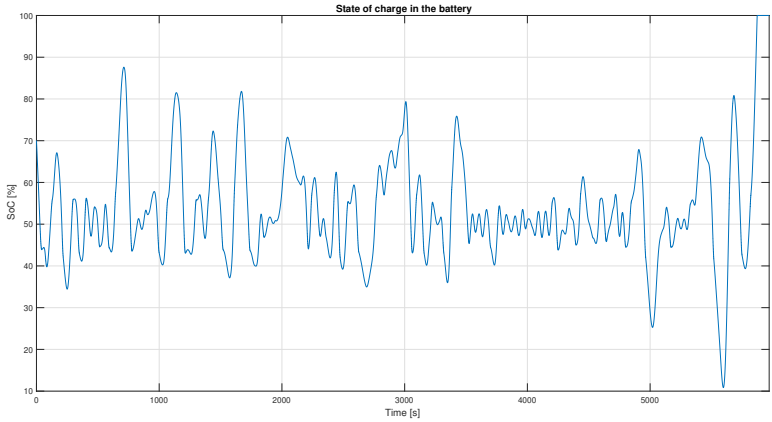

Figure A.3: *Battery state of charge.*

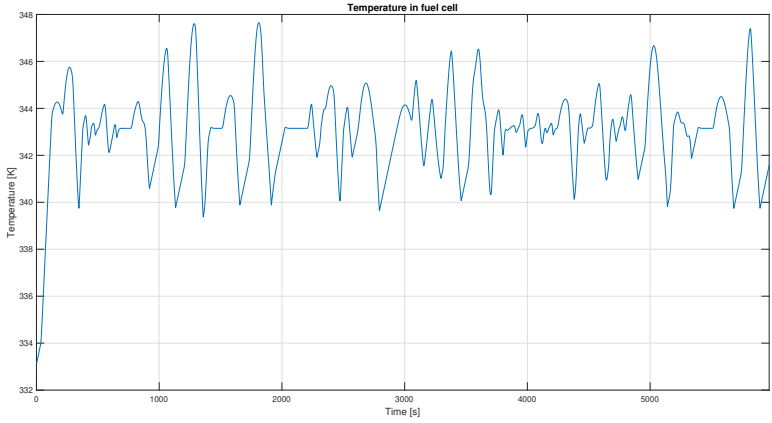

Figure A.4: *Fuel cell temperature.*

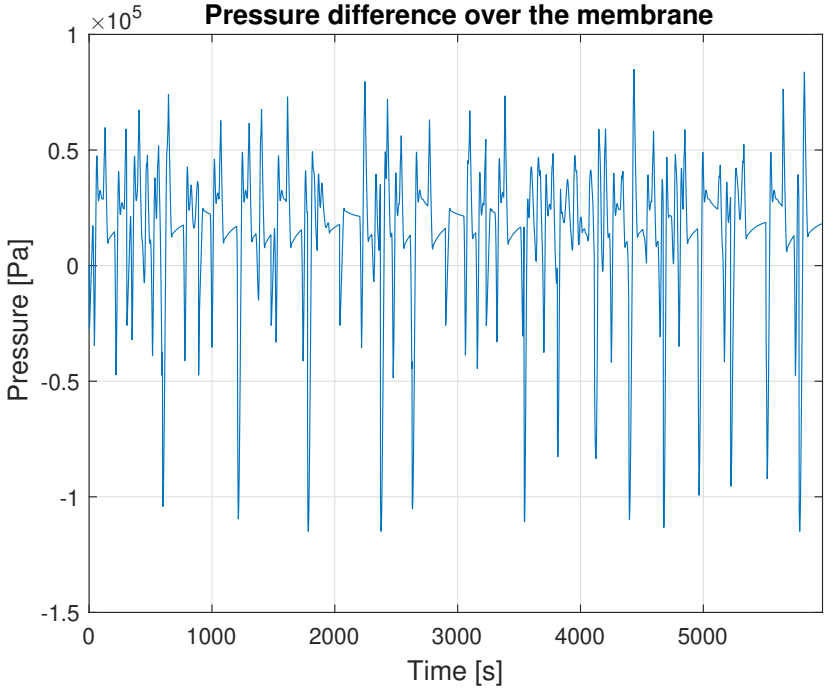

Figure A.5: *The pressure difference over the membrane. A positive value means the anode has the higher pressure, and vice versa.*

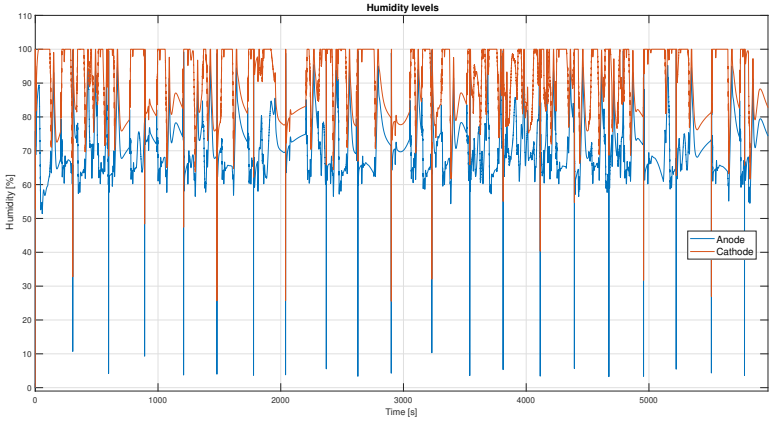

Figure A.6: *The Humidity levels inside the cathode and the anode.*

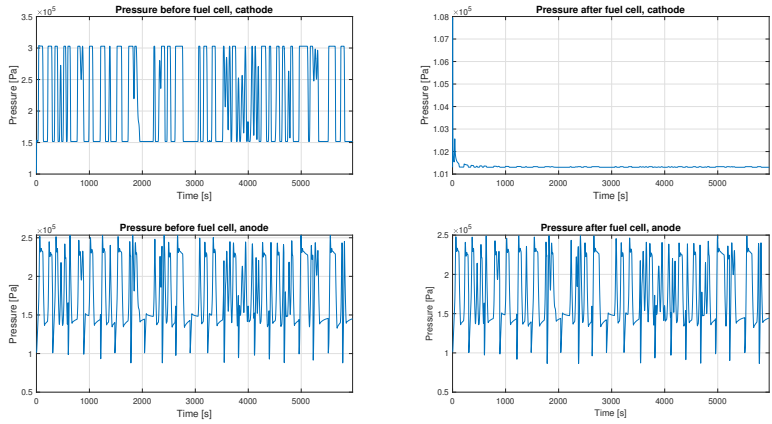

Figure A.7: *The pressure inside the control volumes for the cathode and anode. bf=before, af=after*

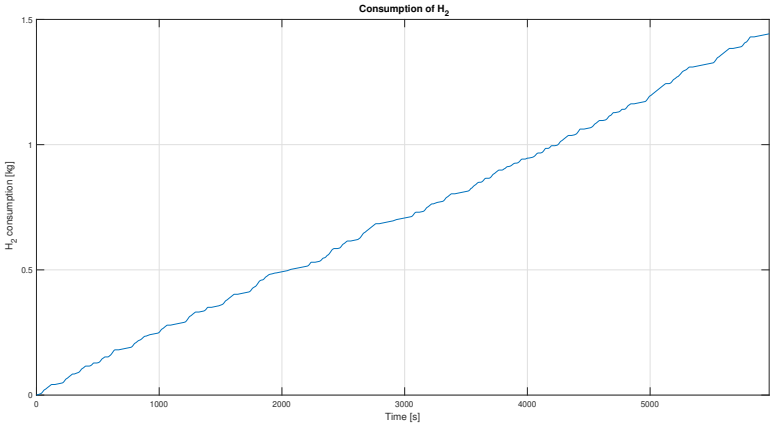

Figure A.8: *Fuel consumption.*

Bibliography

[1] Hydrogen Production: Natural Gas Reforming hydrogen and fuel cell technologies office. https://www.energy.gov/eere/fuelcells/hydrogen-production-natural-gas-reforming#:~:text=Most%20hydrogen%20produced%20today%20in,source%2C%20such%20as%20natural%20gas. Accessed: 2021-05-10.

[2] RK Ahluwalia and X Wang. Buildup of nitrogen in direct hydrogen polymer-electrolyte fuel cell stacks. *Journal of Power Sources*, 171(1):63–71, 2007.

[3] Jong-Woo Ahn and Song-Yul Choe. Coolant controls of a pem fuel cell system. *Journal of Power Sources*, 179(1):252–264, 2008. ISSN 0378-7753. doi: https://doi.org/10.1016/j.jpowsour.2007.12.066. URL https://www.sciencedirect.com/science/article/pii/S037877530702705X.

[4] Lorenzo Bertini. Modeling and optimization of a fuel cell hybrid system, 2011. URL http://kth.diva-portal.org/smash/record.jsf?pid=diva2%3A463510&dswid=1607.

[5] Dariusz Czarkowski. 13 - dc–dc converters. In Muhammad H. Rashid, editor, *Power Electronics Handbook (Third Edition)*, pages 249–263. Butterworth-Heinemann, Boston, third edition edition, 2011. ISBN 978-0-12-382036-5. doi: https://doi.org/10.1016/B978-0-12-382036-5.00013-6. URL https://www.sciencedirect.com/science/article/pii/B9780123820365000136.

[6] Liselott Ericson and Karl-Erik Rydberg. *Pumps and Motors*, pages 33 – 39. Publit, 2018. ISBN 9789177735489.

[7] Lars Eriksson and Lars Nielsen. *Modeling and control of engines and drivelines*. Wiley, 2014. ISBN 9781118479995. URL http://eu.wiley.com/WileyCDA/WileyTitle/productCd-1118479998.html.

[8] Lars Eriksson, Anders Larsson, and Andreas Thomasson. The aac2016 benchmark - look-ahead control of heavy duty trucks on open roads. *IFAC-PapersOnLine*, 49(11):121 – 127, 2016. ISSN 2405-8963. doi: https://doi.org/10.1016/j.ifacol.2016.08.019. URL http://www.sciencedirect.

com/science/article/pii/S2405896316313404. 8th IFAC Symposium on Advances in Automotive Control AAC 2016.

[9] A. Fratta and F. Scapino. Modeling inverter losses for circuit simulation. In *2004 IEEE 35th Annual Power Electronics Specialists Conference (IEEE Cat. No.04CH37551)*, volume 6, pages 4479–4485 Vol.6, 2004. doi: 10.1109/PESC.2004.1354792.

[10] Lino Guzzella and Antonio Sciarretta. *Vehicle Propulsion Systems: Introduction to Modeling and Optimization*. Springer, 01 2007. doi: 10.1007/978-3-642-35913-2.

[11] Shengyan Hou, Jinwu Gao, Yu Zhang, Ming Chen, Jianpeng Shi, and Hong Chen. A comparison study of battery size optimization and an energy management strategy for fchevs based on dynamic programming and convex programming. *International Journal of Hydrogen Energy*, 45(41):21858–21872, 2020. ISSN 0360-3199. doi: https://doi.org/10.1016/j.ijhydene.2020.05.248. URL https://www.sciencedirect.com/science/article/pii/S0360319920321030.

[12] Jianhua Huang. A simple accurate formula for calculating saturation vapor pressure of water and ice. *Journal of applied meteorology and climatology*, 57(6):1265–1272, 2018. ISSN 1558-8424. doi: https://doi.org/10.1175/JAMC-D-17-0334.1. URL https://journals.ametsoc.org/view/journals/apme/57/6/jamc-d-17-0334.1.xml?tab_body=fulltext-display.

[13] Sanggyu Kang, Kyoungdoug Min, and Sangseok Yu. Dynamic modeling of a proton exchange membrane fuel cell system with a shell-and-tube gas-to-gas membrane humidifier. *International Journal of Hydrogen Energy*, 37(7):5866–5875, 2012. ISSN 0360-3199. doi: https://doi.org/10.1016/j.ijhydene.2011.12.063. URL https://www.sciencedirect.com/science/article/pii/S036031991102756X. XII International Symposium on Polymer Electrolytes: New Materials for Application in Proton Exchange Membrane Fuel Cells.

[14] Larisa Karpenko-Jereb and Takuto Araki. Chapter 3 - modeling of polymer electrolyte fuel cells. In Viktor Hacker and Shigenori Mitsushima, editors, *Fuel Cells and Hydrogen*, pages 41 – 62. Elsevier, 2018. ISBN 978-0-12-811459-9. doi: https://doi.org/10.1016/B978-0-12-811459-9.00003-7. URL http://www.sciencedirect.com/science/article/pii/B9780128114599000037.

[15] Andrei A. Kulikovsky. Chapter 4 - quasi-2d model of a fuel cell. In Andrei A. Kulikovsky, editor, *Analytical Modeling of Fuel Cells (Second Edition)*, pages 109 – 192. Elsevier, second edition edition, 2019. ISBN 978-0-444-64222-6. doi: https://doi.org/10.1016/B978-0-44-464222-6.00011-3. URL http://www.sciencedirect.com/science/article/pii/B9780444642226000113.

[16] Andrei A. Kulikovsky. Chapter 3 - one-dimensional model of a fuel cell. In Andrei A. Kulikovsky, editor, *Analytical Modeling of Fuel Cells (Second Edition)*, pages 85 – 108. Elsevier, second edition edition, 2019. ISBN 978-0-444-64222-6. doi: https://doi.org/10.1016/B978-0-44-464222-6.00010-1. URL http://www.sciencedirect.com/science/article/pii/B9780444642226000101.

[17] Yim-Shu Lee and Martin H.L. Chow. 10 - diode rectifiers. In Muhammad H. Rashid, editor, *Power Electronics Handbook (Third Edition)*, pages 149–181. Butterworth-Heinemann, Boston, third edition edition, 2011. ISBN 978-0-12-382036-5. doi: https://doi.org/10.1016/B978-0-12-382036-5.00010-0. URL https://www.sciencedirect.com/science/article/pii/B9780123820365000100.

[18] Vincenzo Liso, Mads Pagh Nielsen, Søren Knudsen Kær, and Henrik H. Mortensen. Thermal modeling and temperature control of a pem fuel cell system for forklift applications. *International Journal of Hydrogen Energy*, 39(16):8410–8420, 2014. ISSN 0360-3199. doi: https://doi.org/10.1016/j.ijhydene.2014.03.175. URL https://www.sciencedirect.com/science/article/pii/S0360319914008672.

[19] Zhiyang Liu, Jian Chen, Hao Liu, Chizhou Yan, Yang Hou, Qinggang He, Jiujun Zhang, and Daniel Hissel. Anode purge management for hydrogen utilization and stack durability improvement of pem fuel cell systems. *Applied Energy*, 275:115110, 2020. ISSN 0306-2619. doi: https://doi.org/10.1016/j.apenergy.2020.115110. URL https://www.sciencedirect.com/science/article/pii/S030626192030622X.

[20] Xavier Llamas and Lars Eriksson. Parameterizing compact and extensible compressor models using orthogonal distance minimization. *Journal of Engineering for Gas Turbines and Power*, 139(1), 2016.

[21] Xavier Llamas and Lars Eriksson. Control-oriented compressor model with adiabatic efficiency extrapolation. In *SAE 2017 World Congress & Exhibition*, number SAE Technical Paper 2017-01-1032, Detroit, MI, USA, April 2017.

[22] Xavier Llamas and Lars Eriksson. Liu cpgui: A toolbox for parameterizing compressor models. (Technical Report Nr. LiTH-ISY-R-3102), 2018. URL http://www.fs.isy.liu.se/en/Publications/Reports/18_R_3102_XL_LE.pdf.

[23] Bertini Lorenzo. Modeling and optimization of a fuel cell hybrid system. 12 2011. URL http://kth.diva-portal.org/smash/record.jsf?pid=diva2%3A463510&dswid=1607.

[24] Yan Ma, Hongyuan Mou, and Haiyan Zhao. Cooling optimization strategy for lithium-ion batteries based on triple-step nonlinear method. *Energy*, 201:117678, 2020. ISSN 0360-5442. doi: https://doi.org/10.

1016/j.energy.2020.117678. URL https://www.sciencedirect.com/science/article/pii/S0360544220307854.

[25] Silvi Octavia Mulyazmi, W.R W Daud and Maria Ulfah. The relative humidity effect of the reactants flows into the cell to increase pem fuel cell performance. 3 2018. doi: https://doi.org/10.1051/matecconf/201815603033.

[26] Vanessa Paladini, Teresa Donateo, Arturo de Risi, and Domenico Laforgia. Super-capacitors fuel-cell hybrid electric vehicle optimization and control strategy development. *Energy Conversion and Management*, 48 (11):3001–3008, 2007. ISSN 0196-8904. doi: https://doi.org/10.1016/j.enconman.2007.07.014. URL https://www.sciencedirect.com/science/article/pii/S0196890407002178. 19th International Conference on Efficiency, Cost, Optimization, Simulation and Environmental Impact of Energy Systems.

[27] Jay T. Pukrushpan, Huei Peng, and Anna G. Stefanopoulou. Control-Oriented Modeling and Analysis for Automotive Fuel Cell Systems. *Journal of Dynamic Systems, Measurement, and Control*, 126(1):14–25, 04 2004. ISSN 0022-0434. doi: 10.1115/1.1648308. URL https://doi.org/10.1115/1.1648308.

[28] Srinivasan Raman, Sathish Swaminathan, Sundaram Bhardwaj, Hemanth Kumar Tanneru, Brian Bullecks, and Raghunathan Rengaswamy. Rapid humidity regulation by mixing of dry and humid gases with feedback control for pem fuel cells. *International Journal of Hydrogen Energy*, 44(1):389–407, 2019. ISSN 0360-3199. doi: https://doi.org/10.1016/j.ijhydene.2018.04.187. URL https://www.sciencedirect.com/science/article/pii/S0360319918314046. State of the Art Materials for Hydrogen Energy.

[29] Uwe Reimer, Werner Lehnert, Yaovi Holade, and Boniface Kokoh. Chapter 2 - irreversible losses in fuel cells. In Viktor Hacker and Shigenori Mitsushima, editors, *Fuel Cells and Hydrogen*, pages 15 – 40. Elsevier, 2018. ISBN 978-0-12-811459-9. doi: https://doi.org/10.1016/B978-0-12-811459-9.00002-5. URL http://www.sciencedirect.com/science/article/pii/B9780128114599000025.

[30] Shemin Sagaria, Rui Costa Neto, and Patricia Baptista. Assessing the performance of vehicles powered by battery, fuel cell and ultra-capacitor: Application to light-duty vehicles and buses. *Energy Conversion and Management*, 229:113767, 2021. ISSN 0196-8904. doi: https://doi.org/10.1016/j.enconman.2020.113767. URL http://www.sciencedirect.com/science/article/pii/S0196890420312905.

[31] Balasubramanian Viswanathan. Chapter 13 - supercapacitors. In Balasubramanian Viswanathan, editor, *Energy Sources*, pages 315–328. Elsevier, Amsterdam, 2017. ISBN 978-0-444-56353-8. doi: https://doi.org/10.1016/

B978-0-444-56353-8.00013-7. URL https://www.sciencedirect.com/science/article/pii/B9780444563538000137.

[32] Z. Yang, D. Patil, and B. Fahimi. Electrothermal modeling of lithium-ion batteries for electric vehicles. *IEEE Transactions on Vehicular Technology*, 68(1):170–179, 2019. doi: 10.1109/TVT.2018.2880138.

[33] Robert H.Turner Yunus A.Cengel, John M.Cimbala. *Fundamentals of Thermal-Fluid Sciences Forth edition*. McGraw-Hill education, 2012. ISBN 9780071325110.

[34] Lei Zhang, Xiaosong Hu, Zhenpo Wang, Fengchun Sun, and David G. Dorrell. A review of supercapacitor modeling, estimation, and applications: A control/management perspective. *Renewable and Sustainable Energy Reviews*, 81:1868–1878, 2018. ISSN 1364-0321. doi: https://doi.org/10.1016/j.rser.2017.05.283. URL https://www.sciencedirect.com/science/article/pii/S1364032117309292.

[35] Weihua Zhang. Chapter 2 - dynamic modeling of coupled systems in the high-speed train. In Weihua Zhang, editor, *Dynamics of Coupled Systems in High-Speed Railways*, pages 55 – 181. Elsevier, 2020. ISBN 978-0-12-813375-0. doi: https://doi.org/10.1016/B978-0-12-813375-0.00002-9. URL http://www.sciencedirect.com/science/article/pii/B9780128133750000029.

[36] Ghassan Zubi, Rodolfo Dufo-López, Monica Carvalho, and Guzay Pasaoglu. The lithium-ion battery: State of the art and future perspectives. *Renewable and Sustainable Energy Reviews*, 89:292–308, 2018. ISSN 1364-0321. doi: https://doi.org/10.1016/j.rser.2018.03.002. URL https://www.sciencedirect.com/science/article/pii/S1364032118300728.